

Physical conditions and chemical abundances in PN M 2-36. Results from deep echelle observations

José N. Espíritu^{1*} & Antonio Peimbert¹

¹*Instituto de Astronomía, Universidad Nacional Autónoma de México, Apdo. Postal 70264, Ciudad de México 04510, México*

Accepted XXX. Received YYY; in original form ZZZ

ABSTRACT

We present a spectrum of the planetary nebula M 2-36 obtained using the Ultra Violet and Visual Echelle Spectrograph (UVES) at the Very Large Telescope (VLT). 446 emission lines are detected. We perform an analysis of the chemical composition using multiple electron temperature (T_e) and density (n_e) diagnostics. T_e and n_e are computed using a variety of methods, including collisionally excited line (CEL) ratios, O⁺⁺ optical recombination lines (ORLs), and measuring the intensity of the Balmer jump. Besides the classical CEL abundances, we also present robust ionic abundances from ORLs of heavy elements. From CELs and ORLs of O⁺⁺, we obtain a new value for the Abundance Discrepancy Factor (ADF) of this nebula, being $ADF(O^{++}) = 6.76 \pm 0.50$. From all the different line ratios that we study, we find that the object cannot be chemically homogeneous; moreover, we find that two-phased photoionization models are unable to simultaneously reproduce critical O II and [O III] line ratios. However, we find a three-phased model able to adequately reproduce such ratios. While we consider this to be a toy model, it is able to reproduce the observed temperature and density line diagnostics. Our analysis shows that it is important to study high ADF PNe with high spectral resolution, since its physical and chemical structure may be more complicated than previously thought.

Key words: ISM: abundances – planetary nebulae: individual: M 2-36.

1 INTRODUCTION

The study of chemical abundances in planetary nebulae (PNe) and H II regions has been mostly based on collisionally excited lines (CELs) of heavy elements, with a sizeable¹ number of objects where optical recombination lines (ORLs) can also be used (see for example Peimbert et al. 2017, and references therein). Where it is possible to determine abundances using both sets, it has been found that chemical abundances estimated from CELs and ORLs yield systematically different values, with those from ORLs always being higher. This difference is quantified by means of the Abundance Discrepancy Factor (ADF) (Liu et al. 2001):

$$ADF(X^{+i}) = \frac{n(X^{+i})_{\text{ORL}}}{n(X^{+i})_{\text{CEL}}}, \quad (1)$$

for ion X^{+i} .

H II regions typically exhibit moderate ADF values, around 2 (e.g. García-Rojas & Esteban 2007; Peña-Guerrero et al. 2012); while in PNe moderate (2–10) and extreme values have been found, some close to 100 (e.g. McNabb et al. 2013).

A number of physical scenarios have been proposed to explain the origin of the abundance discrepancy: thermal inhomogeneities (Peimbert 1967; Peimbert & Costero 1969); coexistence of multiple gas phases with different chemical composition (Liu et al. 2000), notably the case of enrichment by ejecta from central binary stars in PNe

(Corradi et al. 2015; Wesson et al. 2018); non-Maxwellian electron energy distributions (Nicholls et al. 2012, 2013); and varying ionizing radiation fields from short period binary stars (Bautista & Ahmed 2018). Despite these important advances, none of the proposed scenarios has fully reproduced the observed behavior of emission lines and hence the origin of the abundance discrepancy remains an open problem in contemporary astrophysics (García-Rojas et al. 2019).

Traditionally, CELs have been used to estimate the chemical composition of both H II regions and PNe, however the discovery of large ADFs has demanded a rethinking of this approach.

For chemically homogeneous photoionized regions (e.g. almost all known H II regions), ORLs could provide a better representation of the chemical composition in the presence of small thermal inhomogeneities, since ratios of recombination lines are nearly temperature independent (Peimbert & Peimbert 2013); meanwhile, CEL abundances are based on CEL to ORL line ratios which show a strong dependence on temperature.

Nebular abundances play an important role in other fields of astrophysics, such as galactic formation and calibration of strong line methods. For this reason, it is important to find the average or representative chemical composition of a photoionized region, if this can be defined.

In the case of PNe, small ADF values (≤ 5) can be explained by the presence of thermal inhomogeneities (Peimbert et al. 2014); while larger ADFs hint to the presence of chemical inhomogeneities.

It is very likely that the ADF may have a different origin in every object. The real cause may be due to a contribution of most of the proposed physical scenarios. Nonetheless, it is clear that in order to provide insight into this problem, the detection of CELs and

* E-mail: jespiritu@astro.unam.mx

¹ Roger Wesson has compiled a list of objects with measured ADFs: <https://www.nebulousresearch.org/adfs/>

ORLs is desired. Moreover, it may be necessary to develop a detailed photoionization model of the object in question.

M 2-36 is a planetary nebula from the galactic bulge whose ADF was measured to be approximately 5 by [Liu et al. \(2001\)](#). In that work, M 2-36 was studied with medium spectral resolution, using ESO's 1.52 m telescope; effectively resolving ORLs of heavy elements, including C^{++} , N^{++} , and O^{++} . Despite being groundbreaking at the time, recent works on PNe have highlighted the necessity of studying the gas phase with the highest spectral and spatial resolution possible in order to elaborate on the nature of the Abundance Discrepancy Problem. High spectral resolution (with a considerable signal-to-noise ratio) is desirable to detect and fully resolve ORLs, and to compute abundances and physical conditions from them ([Peimbert et al. 2014](#); [McNabb et al. 2016](#)). Intermediate spectral resolution combined with good spatial resolution and detailed analysis (including the use of line-fitting algorithms) has proven to be effective in identifying and characterizing the volumes producing the emission from ORLs and comparing them with CEL emission, providing insight into the nature of the emitting material ([Corradi et al. 2015](#); [García-Rojas et al. 2016](#); [Wesson et al. 2018](#)).

In this work, we present a deep spectral analysis of M 2-36 based on observations from the Ultraviolet and Visual Echelle Spectrograph (UVES), installed at the ESO's 8.2 m Very Large Telescope (VLT). As we will show, the high resolution and spectral coverage ranging from the optical to the near infrared (3030 – 10360 Å) allows the detection of almost 450 emission lines, and a precise calculation of T_e and n_e , which in turn yield chemical abundances with small error bars. The detection of multiple ORLs from heavy elements with a high signal-to-noise ratio has made possible a recalculation of the ADF with small error bars, also allowing us to estimate the physical conditions in the nebula from this set of lines. The latter is important to test the hypothesis that the bulk of the emission of ORLs may arise from cold hydrogen-poor (metal-rich) clumps in the gas phase.

In Section 2 we describe the observations and data reduction. Line identification and extinction correction is presented in Section 3. In Section 4 we present physical conditions. In Section 5 we compute ionic and total abundances. In Section 6 we discuss the presence of inhomogeneities in the nebula, leading us to discuss photoionization models in Section 7. Finally, in Section 8 we present our summary and conclusions.

2 OBSERVATIONS

The observations were carried out during the night of March 30, 2003 (programme ID 70.C-0008(A)), using the Ultraviolet and Visual Echelle Spectrograph (UVES; [D'Odorico et al. \(2000\)](#)) installed at the Very Large Telescope in Cerro Paranal, Chile. We observed the object simultaneously with the red and blue arms in two settings covering effectively the range from 3030 to 10360 Å, except for small gaps resulting from the separation between the two CCDs used in the red arm. In all, unusable wavelength ranges were 5780–5830, 8530–8640, 10084–10090, and 10250 – 10360 Å. The slit dimensions were set to $2'' \times 10''$, with an East-West orientation, effectively covering M 2-36 (Fig. 1) while avoiding the central star. The resolving power with this configuration was $\Delta\lambda/\lambda \sim 30000$. The atmospheric dispersion corrector was used to keep the same observed region within the slit, regardless of the airmass value. Data were acquired according to the observation plan detailed in Table 2.

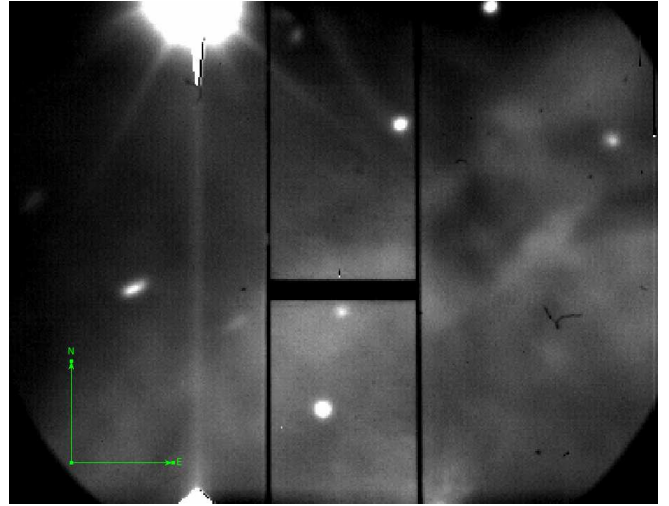


Figure 1. Slit position across M 2-36. Its dimensions are 2×10 arcsec².

The spectra were reduced using IRAF² following the standard procedure of bias subtraction, aperture extraction, flat fielding, wavelength calibration and flux calibration. For the latter, standard stars EG 274 and CD-329927 were observed.

3 LINE FLUXES, IDENTIFICATION AND EXTINCTION CORRECTION

The reduced spectrum was analyzed using IRAF's *splot* routine. The flux of the emission lines was determined by integrating between two points over the local continuum estimated by eye. When dealing with line blends, a gaussian profile was fitted using *splot*, considering the laboratory wavelength as reference, allowing the actual wavelength to shift while keeping the separation constant.

Some lines exhibit a double peak due to nebular expansion; in these cases, the average wavelength of the two components was used for identification, and the corresponding flux was calculated by integrating both peaks. 446 emission lines were identified, based on previous identifications by [Liu et al. \(2001\)](#) and the Atomic Line List v2.05b21 ([van Hoof 2018](#)). Table 20 presents the results of our identifications: in Column 1 we present the laboratory wavelength λ_0 for air; Column 2 presents the ion emitting the line; Column 3 shows the multiplet originating the emission; Column 4 shows the flux corrected for reddening relative to $H(\beta)$, $I(H\beta)$. The second to last column includes the fractional error (1σ) of the line intensities in percentage. Dubious identification is noted with a question mark.

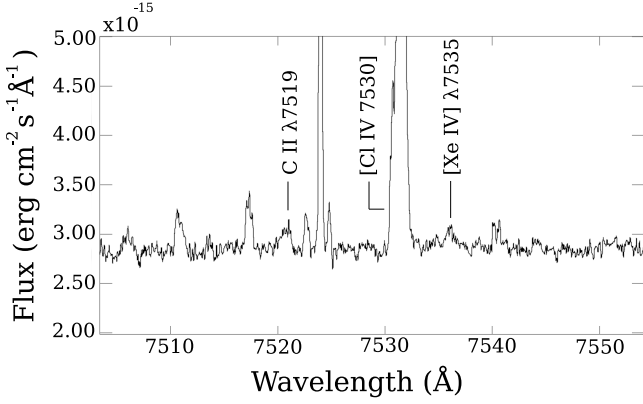
Notably we have resolved over forty recombination lines of $O\ II$, including the entirety of multiplet V1, which is central to study the ADF(O^{++}). We have also identified three emission features corresponding to $[Kr\ IV]$, and $[Xe\ IV]$, (Figure 2) which are produced by the s-process (slow neutron capture process); making these detections the first ones of neutron capture lines in PN M 2-36.

The theoretical intensity ratios for the Balmer and Paschen emission lines were calculated using the program INTRAT by [Storey & Hummer \(1995\)](#) considering a constant electron temperature $T_e = 8000$ K, and an electron density $n_e = 5000$ cm⁻³; there

² IRAF is distributed by NOAO, which is operated by AURA, Inc., under cooperative agreement with NSF.

Table 1. Journal of observations

| Cross Disperser | Dichroic | λ (\AA) | Exp. time (s) | Identification |
|-----------------|----------|----------------------------|----------------|------------------|
| 1 | 1 | 3100 – 3880 | 5×225 | UV |
| 2 | 2 | 3730 – 4990 | 3×675 | BLUE |
| 3 | 1 | 4760 – 6840 | 3×225 | GREEN / RED |
| 4 | 2 | 6600 – 10360 | 3×675 | NEAR IR / FAR IR |


Figure 2. [Xe IV] detected in our spectra, emitted by an ion created from the s-process.

was no need to modify these values since hydrogen lines are nearly independent of temperature and density. These theoretical values were compared to our measurements in order to estimate the extinction correction.

We adopted the extinction law of Cardelli et al. (1989). The logarithmic extinction correction for $H\beta$, $C(H\beta)$, and the ratio of total to selective extinction, R_V , were fitted simultaneously and determined by reducing the quadratic discrepancies between the theoretical and measured H lines in units of the expected error, χ^2 . The fluxes were normalized with respect to the Balmer decrement, meaning that the value of $I(H\beta)$ was allowed to deviate slightly from 100. The best fit parameters correspond to $C(H\beta)=0.33 \pm 0.01$ and $R_V = 2.75$. The error contribution from flux calibration was estimated to be 1.5%.

The line fluxes were extinction corrected according to

$$I(\lambda) = 10^{C(H\beta)f(\lambda)} F(\lambda). \quad (2)$$

Where $f(\lambda)$ is the extinction curve for $R_V = 2.75$.

4 PHYSICAL CONDITIONS

4.1 Physical conditions from CELs

Electron temperatures and densities obtained from various plasma diagnostics are presented in Table 2. We have made the distinction between high-ionization and low-ionization species, and assigned a respective electron temperature and density for each. Individual diagnostics were computed using PyNeb’s *getCrossTemden* routine (Luridiana et al. 2015), allowing a simultaneous determination of T_e and n_e ; the results are plotted in Figure 3. For [O III] we have considered the nebular to auroral line ratio $\lambda 4959/\lambda 4363$, excluding [O III] $\lambda 5007$ since it was slightly saturated in our spectra. The adopted T_e and n_e for each ionization zone were obtained from the weighted average of the diagnostics considered. The atomic data set used is listed in Table 4.

Errors associated to T_e and n_e were propagated from intensity errors using Monte Carlo simulations. We generated 500 random values for each observed line intensity, considering a Gaussian distribution centered on said intensity. We verified that for larger random samples, the errors remained stable.

Escalante et al. (2012) have pointed that O II emission lines, such as those from multiplet V1, may be affected by fluorescence in low excitation planetary nebulae such as IC 418. We have considered these effects to be negligible in M 2-36 since its ionization degree is much higher than that of IC 418.

[N II] $\lambda 5755$ is known to be affected by recombination emission. Thus, the intensity was corrected using Equation 1 from Liu et al. (2000), amounting to 3%. [O II] $\lambda\lambda 7320+7330$ is affected by recombination too; using Equation 2 from Liu et al. (2000) we find the recombination contribution to be 7%. Both sets of lines were corrected before computing the physical conditions reported in Table 2.

Our calculations are consistent with those reported by Liu et al. (2001) in their study of M 2-36, except for the case of [N II] $\lambda\lambda 6548+6583/\lambda 5755$. This difference cannot be attributed to the recombination contribution to the lines of [N II] since it is very small. It must be noted that our $T_e([N II])$ is consistent with our $T_e([O II])$ determination within 2σ , while the temperatures by Liu et al. are not consistent; on the other hand, our low-ionization temperatures are much higher than our high-ionization temperatures, while only the $T_e([O II])$ is high in that work. We must also note that our measured flux for [N II] $\lambda 5755$ is considerably higher than the one reported by Liu et al. Another possible reason for the discrepancy is that it arises from the fact that we are observing different volumes within the nebula: since we observe an area of $2'' \times 10''$ and Liu et al. study the whole nebula we do not expect all quantities to be equal. In any case, the available data does not allow us to go deeper into the causes of the difference in $T_e([N II])$.

4.2 Physical conditions from ORLs

Electron temperatures and densities can be obtained from ORLs of H^+ , He^+ and O^{++} .

$T_e(H^+)$ is usually obtained from the Balmer Jump discontinuity. In Figure 4 we show the spectrum near the discontinuity. By fitting gaussian profiles to the spectrum, using IRAF’s *splot* routine, we have resolved H I recombination lines up to H36. The electron temperature can be computed from Equation 3 of Liu et al. (2001),

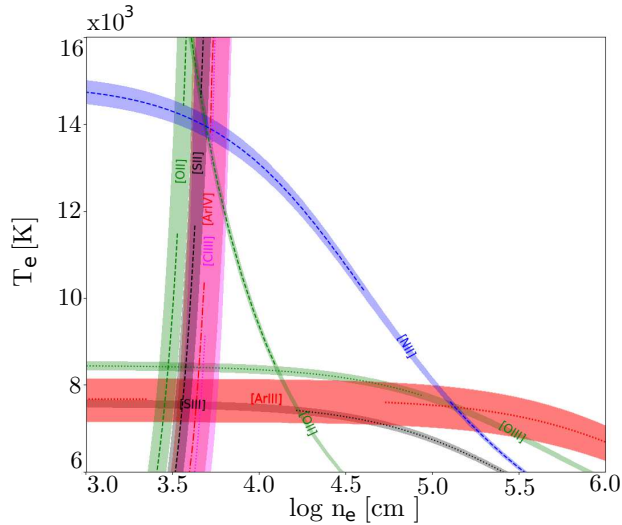
$$T_e = 368 \times (1 + 0.259y^+ + 3.409y^{++}) \left(\frac{BJ}{H11} \right)^{-3/2} \text{ K}, \quad (3)$$

yielding a value of 6100 ± 900 K, which is in agreement with the previous determination by Liu et al. (2001). We will refer to this value as $T_e(BJ)$.

T_e can be obtained from the ratio of O II to [O III] lines, while the ratio of O II $\lambda 4649/V1$ yields n_e . Comparing the intensity of multiplet V1 of O II to [O III] $\lambda 4959$ and using equation (1) from Peimbert et al.

Table 2. Temperatures and densities from forbidden line ratios

| Diagnostic | T_e (K) | Diagnostic | n_e (cm^{-3}) |
|--|-----------------|---|----------------------------|
| High Ionization | | | |
| [O III] $\lambda\lambda 4959/\lambda 4363$ | 8380 ± 100 | [Cl III] $\lambda 5517/\lambda 5537$ | 6530 ± 1800 |
| [S III] $\lambda\lambda 9069 + 9532/\lambda 6312$ | 7600 ± 150 | [Ar IV] $\lambda\lambda 711/\lambda 4740$ | 4900 ± 1100 |
| [Ar III] $\lambda\lambda 7136 + 7751/\lambda 5192$ | 7650 ± 500 | | |
| Adopted | 8130 ± 100 | | 5400 ± 1000 |
| Low ionization | | | |
| [N II] $\lambda\lambda 6548 + 6583/\lambda 5755$ | 14200 ± 300 | [O II] $\lambda 3726/\lambda 3729$ | 3700 ± 600 |
| [O II] $\lambda\lambda 3726 + 3729/\lambda\lambda 7320 + 7330$ | 15100 ± 400 | [S II] $\lambda 6716/\lambda 6731$ | 3400 ± 500 |
| Adopted | 14500 ± 300 | | 3500 ± 600 |

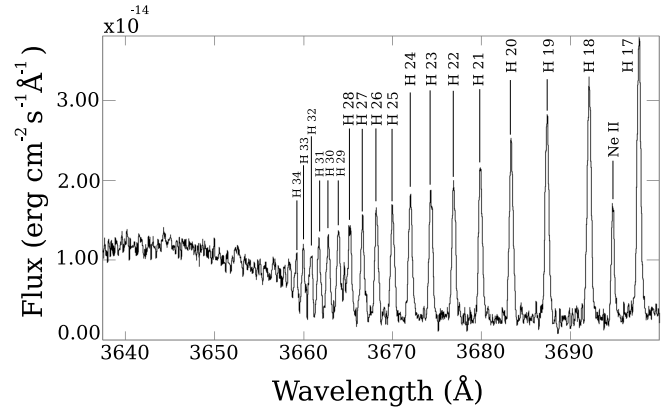
**Figure 3.** Electron temperature and density diagnostics from forbidden line ratios.

(2014), we find that $T_e = 5400 \pm 400$ K. We also estimated n_e from Figure 3 of Peimbert & Peimbert (2013), obtaining $n_e = 1100 \pm_{600}^{1000} \text{cm}^{-3}$. We will refer to these quantities as $T_e(\text{V1}/4959)$ and $n_e(\text{V1})$.

He I lines can provide an estimation of T_e and n_e . From the intensity ratio of He I $\lambda 7281/\lambda 6678$, and Figure 2 of Zhang et al. (2005), we estimate $T_e(\text{He I}) = 5400$ K. Similarly, we have estimated T_e using HELIO14 (Peimbert et al. 2012) and found $T_e(\text{He I}) = 7500$ K (note that for this estimation, we have to set $t^2 = 0.00$ in the code). Note that in the work of Zhang, the authors find a value of 2790 ± 1000 K. They also find $T_e(\text{He I})$ to be systematically lower than $T_e(\text{BJ})$ in all but one object out of a sample of fifty PNe. Our result thus contradicts the one reported by Zhang et al. (2005); this will be explored further in Section 7.

Physical conditions from ORLs are summarized in Table 3.

It is remarkable that temperatures derived from heavy element ORLs are systematically lower than those derived from CELs. This is consistent with the results obtained by Peimbert et al. (2014) in PNe, however the difference between $n_e(\text{V1})$ appears to be significantly larger than the average found in their sample. $n_e(\text{V1})$ is irreconcilable with $n_e[\text{Cl III}]$ and any other CEL diagnostic; this will be addressed in section 7.

**Figure 4.** Balmer decrement from our observations.**Table 3.** Physical conditions from ORLs

| Method | T_e (K) | n_e (cm^{-3}) |
|-----------------------------------|----------------|----------------------------|
| H I Balmer Jump, $T_e(\text{BJ})$ | 6100 ± 900 | |
| He I $\lambda 7281/\lambda 6678$ | 5400 | |
| He I (HELIO 14) | 7500 | 6380 ± 1500 |
| O II (V1) | | $1100 \pm_{600}^{1000}$ |
| O II (V1/ $\lambda 4959$) | 5400 ± 400 | |

5 CHEMICAL ABUNDANCES

5.1 Ionic abundances from collisionally excited lines

We have computed the ionic abundances from multiple CELs of heavy elements. All computations were performed with PyNeb considering the atomic data from Table 4. Errors were propagated from those associated to line intensities using Monte Carlo simulations. As explained in section 4.1, we have used a two-zone scheme, distinguishing between species originating mainly in the high ionization zones (O^{++} , Ne^{++} , S^{++} , Cl^{++} , Cl^{3+} , Ar^{++} , Ar^{3+} , Kr^{3+} , and Xe^{3+}) and those that originate in the low ionization zones (N^0 , N^+ , O^0 , O^+ , S^+ and Cl^+). Our results are presented in Table 5.

5.2 Ionic abundances from recombination lines

We have detected 58 He I and 8 He II lines in our spectrum. Most of the helium found in the observed volume is singly ionized.

The He^+/H^+ ratio was computed from 9 lines using the package HELIO14, an update of the software described in Peimbert et al. (2012). This package uses a maximum likelihood method to fit simul-

Table 4. Atomic data set used for collisionally excited lines.

| Ion | Transition probabilities | Collisional strengths |
|------------------|---|-------------------------------|
| N ⁰ | Wiese et al. (1996) | Pequignot & Aldrovandi (1976) |
| N ⁺ | Froese Fischer & Tachiev (2004) | Tayal (2011) |
| O ⁰ | Wiese et al. (1996) | Pequignot & Aldrovandi (1976) |
| O ⁺ | Froese Fischer & Tachiev (2004) | Kisielius et al. (2009) |
| O ⁺⁺ | Froese Fischer & Tachiev (2004) Storey & Zeippen (2000) | Storey et al. (2014) |
| Ne ⁺⁺ | Galavis et al. (1997) | McLaughlin & Bell (2000) |
| S ⁺ | Podobedova et al. (2009) | Tayal & Zatsarinny (2010) |
| S ⁺⁺ | Podobedova et al. (2009) | Tayal & Gupta (1999) |
| Cl ⁺ | Mendoza & Zeippen (1983) | Tayal (2004) |
| Cl ⁺⁺ | Mendoza & Zeippen (1983) | Butler & Zeippen (1989) |
| Cl ³⁺ | Kaufman & Sugar (1986) Mendoza & Zeippen (1982a) Ellis & Martinson (1984) | Galavis et al. (1995) |
| Ar ⁺⁺ | Mendoza & Zeippen (1983) Kaufman & Sugar (1986) | Galavis et al. (1995) |
| Ar ³⁺ | Mendoza & Zeippen (1982b) | Ramsbottom & Bell (1997) |
| Kr ³⁺ | Biémont & Hansen (1986) | Schoning (1997) |
| Xe ³⁺ | Biémont et al. (1995) | Schoening & Butler (1998) |

Table 5. Ionic abundances from collisionally excited lines

| Ion | $t^2 = 0.00$ |
|------------------|--------------|
| N ⁰ | 5.59 ± 0.05 |
| N ⁺ | 7.10 ± 0.04 |
| O ⁰ | 6.60 ± 0.03 |
| O ⁺ | 6.96 ± 0.04 |
| O ⁺⁺ | 8.79 ± 0.02 |
| Ne ⁺⁺ | 8.30 ± 0.03 |
| S ⁺ | 5.64 ± 0.04 |
| S ⁺⁺ | 6.92 ± 0.03 |
| Cl ⁺ | 3.84 ± 0.08 |
| Cl ⁺⁺ | 5.28 ± 0.05 |
| Cl ³⁺ | 4.72 ± 0.04 |
| Ar ⁺⁺ | 6.48 ± 0.04 |
| Ar ³⁺ | 5.97 ± 0.04 |
| Kr ³⁺ | 3.30 ± 0.11 |
| Xe ³⁺ | 2.70 ± 0.15 |

Table 6. Atomic data used for recombination lines.

| Ion | Recombination coefficients |
|------------------|----------------------------|
| H ⁺ | Storey & Hummer (1995) |
| He ⁺ | Porter et al. (2012, 2013) |
| He ⁺⁺ | Storey & Hummer (1995) |
| C ⁺⁺ | Davey et al. (2000) |
| N ⁺⁺ | Fang et al. (2011) |
| O ⁺⁺ | Storey et al. (2017) |
| Ne ⁺⁺ | Kisielius et al. (1998) |

taneously He⁺/H⁺; electron density; the optical depth of He I λ 3889, τ_{3889} ; the normalized mean square thermal inhomogeneity, t^2 ; and T_0 . One of the main advantages of this software is the precise calculation it produces, with an accuracy of up to three significant figures. Results are presented in Table 9.

For He⁺⁺/H⁺, the only two lines not contaminated by emission from other ions that present errors lower than 15% are He II λ 4686

Table 7. Ne⁺⁺/H⁺ ionic abundances from optical recombination lines

| λ_0 | 12+log(Ne ⁺⁺ /H ⁺) |
|----------------|---|
| 3694.21 | 9.02 ± 0.06 |
| 3709.62 | 8.98 ± 0.08 |
| 3766.26 | 8.60: |
| 3777.14 | 8.82: |
| Adopted | 9.00 ± 0.08 |

Table 8. N⁺⁺/H⁺ abundances from recombination lines

| λ_0 | Mult. | 12+log(N ⁺⁺ /H ⁺) |
|----------------|--------------------|--|
| 4035.08 | V39a | 9.26 ± 0.08 |
| 4041.31 | V39b | 9.21 ± 0.06 |
| 4043.53 | V39a | 9.11 ± 0.10 |
| 4607.16 | V5 | 8.84 ± 0.14 |
| 4621.39 | V5 | 9.06 ± 0.11 |
| 4630.54 | V5 | 9.16 ± 0.05 |
| 4643.09 | V5 | 8.78 ± 0.13 |
| 4788.13 | V20 | 8.64 ± 0.17 |
| 5495.67 | 3P-3P ₀ | 8.70 ± 0.16 |
| 5666.63 | V3 | 9.14 ± 0.05 |
| 5676.02 | V3 | 9.09 ± 0.08 |
| 5679.56 | V3 | 9.20 ± 0.03 |
| 5686.21 | V3 | 9.14 ± 0.10 |
| 5710.77 | V3 | 9.21 ± 0.08 |
| 5927.81 | 3P-3D ₀ | 8.67 ± 0.11 |
| Adopted | | 9.16 ± 0.09 |

and He II λ 3203. We have adopted the value derived from He II λ 4686 since it is the strongest one.

Besides H I, He I, and He II, we have detected several ORLs produced by C⁺⁺, N⁺⁺, O⁺⁺ and Ne⁺⁺. We have computed ionic abundances for all of them considering the high ionization T_e and n_e , and the atomic data from Table 6; they are presented in Tables 7, 8, 10 and 11. For Ne⁺⁺ we adopted the weighted average of λ 3694.21 and

Table 9. He⁺/H⁺ and He⁺⁺/H⁺ from ORL

| λ_0 | $12 + \log(\text{He}^+/\text{H}^+)$ |
|-----------------------|--|
| 3819 | 11.091 |
| 3889 | 11.101 |
| 4388 | 11.089 |
| 4471 | 11.125 |
| 4713 | 11.114 |
| 4922 | 11.068 |
| 5876 | 11.083 |
| 6678 | 11.144 |
| 7065 | 11.102 |
| Adopted | 11.101 ± 0.004 |
| λ_0 | $12 + \log(\text{He}^{++}/\text{H}^+)$ |
| 4686 (adopted) | 9.52 ± 0.02 |

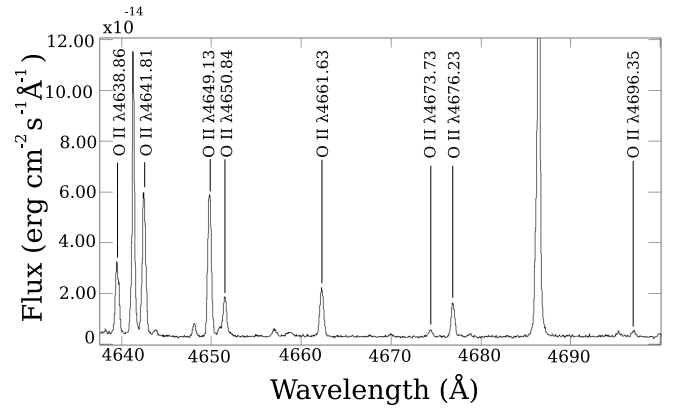
$\lambda 3709.62$; for N⁺⁺ we adopted the weighted average from multiplet V5 lines.

Special attention has been dedicated to recombination lines of O II, of which we have detected all lines that make up multiplet V1, namely O II $\lambda 4638.86$, $\lambda 4641.81$, $\lambda 4649.13$, $\lambda 4650.84$, $\lambda 4661.63$, $\lambda 4673.73$, $\lambda 4676.23$, and $\lambda 4696.35$. All lines were detected with a considerable signal-to-noise ratio allowing us to compute the ionic abundance with small errors (Table 11). We have adopted the abundance obtained from the weighted average of multiplet V1. In Figure 5 we show the quality of the spectrum around this multiplet.

O II lines from other multiplets are also found in our spectrum. We have selected those with reasonable errors (no greater than 30%) in order to compute O⁺⁺/H⁺, also we have been careful not to include lines that may be contaminated by those from other ions.

Table 11 highlights that 3d-4f transitions yield systematically larger values for O⁺⁺/H⁺ than those derived from multiplet V1. Peimbert & Peimbert (2013) have argued that O II $\lambda 4089.29$ may be contaminated by Si IV $\lambda 4088.86$, meaning the value derived for O⁺⁺ from this line could be overestimated. In our spectrum, Si IV $\lambda 4088.86$ should be present at $\lambda 4089.30$; we have verified that there is a feature present on the blue side of O II $\lambda 4089.29$. While the wavelength is consistent with Si IV $\lambda 4088.86$, recent work by Méndez-Delgado et al. (2021) shows that the feature registered by Peimbert & Peimbert (2013) is also consistent with an artifact arising from internal reflections in dichroic #2 in the blue arm of UVES. On the other hand, we identify a weak feature at $\lambda 4116.74$ which is produced by the same multiplet of Si IV, strengthening the possibility of the presence of Si IV $\lambda 4088.86$; neither of the features can be measured well enough to determine their ratio with any confidence nor is it possible to determine the abundance of Si⁺⁺ from Si IV $\lambda 4116.74$. Therefore we cannot establish firmly whether the feature at $\lambda 4089.30$ is produced by Si IV or an internal reflection.

For the case of C⁺⁺, Grandi (1976) recommends using the lines that populate C II $\lambda 4267.15$, therefore we have considered the weighted average of the abundances listed in Table 10. We have used the recombination coefficients by Davey et al. (2000), considering case B recombination for the temperature range $T_e = 2500\text{--}30000$ K, and electron density $n_e = 10^4 \text{ cm}^{-3}$. Our values agree with the results obtained by Liu et al. (2001).

**Figure 5.** Spectrum around multiplet V1 of O II**Table 10.** C⁺⁺/H⁺ from optical recombination lines

| λ_0 | Mult. | $12 + \log(\text{C}^{++}/\text{H}^+)$ |
|----------------|-------|---------------------------------------|
| 4267.15 | 6 | 9.34 ± 0.06 |
| 5342.38 | 17.06 | 9.32 ± 0.08 |
| 6151.43 | 16.04 | 9.22 ± 0.06 |
| 6461.95 | 17.04 | 9.36 ± 0.04 |
| 9903.46 | 17.02 | 9.45 ± 0.03 |
| Adopted | | 9.36 ± 0.03 |

5.3 Total abundances

In order to compute total elemental abundances, ionic abundances have to be corrected for the presence of unobserved ions in the gas. This is done by means of an Ionization Correction Factor (ICF). Total abundances for M 2-36 are reported in Table 12.

For O, Ne, S, and Ar we used the ICFs developed by Delgado-Inglada et al. (2014) through photoionization models of PNe.

Since we detect several He II lines and $\omega = \text{O}^{++}/(\text{O}^+ + \text{O}^{++}) = 0.98$, we have to account for the presence of O³⁺ when computing O/H.

Delgado-Inglada et al. (2014) recommend not to use their ICF for N when $\omega \geq 0.95$ and in turn we refer to the one proposed by Kingsburgh & Barlow (1994), which assumes that N/O = N⁺/O⁺.

We detect Cl⁺, Cl⁺⁺ and Cl³⁺ in our spectrum of M 2-36, therefore we can obtain Cl/H by adding their ionic abundances. We have also computed Cl/H using the ICF provided by Liu et al. (2000); yielding a value smaller than the direct sum by 0.28 dex. We do not use Delgado-Inglada et al. (2014) ICF in this case since it is only valid when $0.02 \leq \omega \leq 0.95$. We have adopted the value obtained from the direct sum.

Regarding neutron capture elements, only [Kr IV] $\lambda 5867.74$ and [Xe IV] $\lambda 7535.40$ are fully resolved, therefore we have considered them using equation (3) of Sterling et al. (2015), from which we compute both Kr/H and Xe/H, given the similar ionization potential of Kr³⁺ and Xe³⁺.

Abundances derived from observations are consistent with a Peimbert Type I PN, according to the criterion first stated by Peimbert (1978) and later refined by Peimbert & Torres-Peimbert (1983) that requires He/H ≥ 0.125 and N/O ≥ 0.5 . Kingsburgh & Barlow (1994) proposed that Type I PNe can be defined from the ratio of N/O alone; based on recent photoionized region and solar abundances,

Table 11. O⁺⁺/H⁺ ionic abundances from optical recombination lines

| Mult. | λ_0 | $12 + \log(\text{O}^{++}/\text{H}^+)$ |
|--------------------------|-------------|---------------------------------------|
| V1 | 4638.86 | 9.75 ± 0.04 |
| V1 | 4641.81 | 9.72 ± 0.02 |
| V1 | 4649.13 | 9.56 ± 0.03 |
| V1 | 4650.84 | 9.53 ± 0.04 |
| V1 | 4661.63 | 9.57 ± 0.04 |
| V1 | 4673.73 | 9.48 ± 0.11 |
| V1 | 4676.23 | 9.55 ± 0.05 |
| V1 | 4696.35 | 9.72 ± 0.12 |
| V1 sum (adopted) | | 9.62 ± 0.03 |
| <hr/> | | |
| V2 | 4317.14 | 9.48 ± 0.08 |
| V2 | 4319.63 | 9.52 ± 0.08 |
| V2 | 4325.76 | 9.49 ± 0.15 |
| V2 | 4345.56 | 9.43 ± 0.07 |
| V2 | 4349.43 | 9.55 ± 0.14 |
| V2 | 4366.89 | 9.54 ± 0.10 |
| V2 sum | | 9.50 ± 0.05 |
| <hr/> | | |
| V5 | 4414.90 | 9.47 ± 0.07 |
| V5 | 4416.97 | 9.50 ± 0.08 |
| V5 sum | | 9.48 ± 0.06 |
| <hr/> | | |
| V10 | 4069.88 | 9.74 ± 0.03 |
| V10 | 4072.16 | 9.63 ± 0.03 |
| V10 | 4075.86 | 9.76 ± 0.03 |
| V10 | 4078.84 | 9.48 ± 0.10 |
| V10 | 4085.11 | 9.52 ± 0.08 |
| V10 | 4092.93 | 9.59 ± 0.09 |
| V10 sum | | 9.70 ± 0.05 |
| <hr/> | | |
| V19 | 4121.46 | 9.41 ± 0.10 |
| V19 | 4132.80 | 9.40 ± 0.08 |
| V19 | 4153.30 | 9.52 ± 0.06 |
| V19 | 4156.53 | 10.03 ± 0.08 |
| V19 | 4169.22 | 9.71 ± 0.08 |
| V19 sum | | 9.56 ± 0.05 |
| <hr/> | | |
| V20 | 4110.79 | 9.67 ± 0.08 |
| V20 | 4119.22 | 9.58 ± 0.05 |
| V20 sum | | 9.60 ± 0.04 |
| <hr/> | | |
| V25 | 4699.22 | 9.64 ± 0.16 |
| V25 | 4705.35 | 9.67 ± 0.14 |
| V25 sum | | 9.66 ± 0.11 |
| <hr/> | | |
| 3d-4f transitions | | |
| V48a | 4071.23 | 9.78 ± 0.09 |
| V48a | 4089.29 | 9.74 ± 0.04 |
| V48b | 4083.90 | 9.56 ± 0.08 |
| V50a | 4062.94 | 10.08 ± 0.08 |
| V53b | 4294.78,92 | 9.55 ± 0.08 |
| V86a | 4491.23 | 9.68 ± 0.09 |
| V92a | 4609.44 | 9.74 ± 0.06 |
| V92b | 4602.13 | 9.83 ± 0.07 |
| V92c | 4610.20 | 10.03 ± 0.07 |

Henry et al. (2004) have established a value of N/O ≥ 0.65 for Type I PNe. We obtain He/H = 0.129 and N/O = 1.44, implying that M 2-36 is a strong Type I PN.

Our ORL abundances for He and C agree with those of Liu et al. (2001) and Ratag et al. (1997) within 1σ (see Table 13). Nonetheless, there is a significant difference between CEL abundances of O and N; our Ne/H determination agrees with that of Ratag et al., but not with Liu et al. This is to be expected because, as we will see in sec-

Table 12. Total abundances.

| | ICF | CELS ^a | ORL |
|----|---|------------------------|--------------------------|
| He | He ⁺ + He ⁺⁺ | | 11.112 ± 0.008 |
| C | Assuming C/O = C ⁺⁺ /O ⁺⁺ | | 9.36 ± 0.10 |
| N | Kingsburgh & Barlow (1994) | 8.95 ± 0.06 | 9.17 ± 0.11 ^b |
| O | Delgado-Inglada et al. (2014) | 8.79 ± 0.03 | 9.64 ± 0.04 |
| Ne | Delgado-Inglada et al. (2014) | 8.37 ± 0.06 | 9.02 ± 0.07 |
| | Peimbert & Costero (1969) | 8.36 ± 0.05 | |
| S | Delgado-Inglada et al. (2014) | 7.35 ± $^{0.2}_{0.12}$ | |
| | Stasińska (1978) | 6.94 ± 0.05 | |
| Cl | Cl ⁺ + Cl ⁺⁺ + Cl ³⁺ | 5.41 ± 0.08 | |
| | Liu et al. (2000) | 5.68 ± 0.10 | |
| Ar | Delgado-Inglada et al. (2014) | 6.77 ± 0.7 | |
| Kr | Sterling et al. (2015) | 3.44 ± 0.15 | |
| Xe | Sterling et al. (2015) | 2.83: | |

^a Abundances determined with $r^2 = 0.00$.

^b Assuming N/O = N⁺⁺/O⁺⁺ (ORLs).

Colons indicate very uncertain abundances.

tions 6 and 7, this object is composed from several notably different components; under such conditions it would be very unlikely to find uniform chemical abundance determinations between observations that do not include the emission from the entire object.

5.4 Abundance Discrepancy Factors

Our ADF values are presented in Table 14. For ADF(O⁺⁺), our value of 6.76 ± 0.50 is somewhat higher than the global ADF obtained from Liu et al. (2001), taking O II V1 and optical [O III] abundances as reference, which is ~5.50. Nonetheless, the ADF value can change depending on the methodology used. The small differences may be due to the fact that the two works use slightly different methodologies, and different zones of the object have been analyzed. Also we must note that previous works on the ADF in PN M 2-36 do not include error bars.

Although it has been found that some PNe with ADF ≤ 8 or similar can be chemically homogeneous, this is not a strict discriminator. Some of the parameters exhibited by M 2-36 suggest that it is not chemically homogeneous, notably, the irreconcilable values obtained for r^2 (further discussed in Section 6), as well as the large difference in T_e and n_e between high and low ionization stages.

6 INHOMOGENEITIES

The existence of the ADF means that homogeneous single-phase models do not reproduce PNe adequately, implying the existence of inhomogeneities in either chemical composition, density, and/or temperature (see Peimbert et al. 2017, and references therein). Regarding the density inhomogeneities, while the filling factor is well known, (see Osterbrock 1974, and subsequent editions) it will not result in an ADF; in order to produce large ADFs, the inhomogeneities needed include clumps with $n_e \geq 100\,000\text{ cm}^{-3}$ as well as a surrounding volume with densities in the few thousands; in the remaining of this paper, this is what we will be referring to when we make reference to density inhomogeneities. Two important open questions remain: what is the relevance of each of the possible sources of inhomogeneity? and, what is the physical size of the relevant inhomogeneities?

It must be noted that inhomogeneities in either density or chemical composition will also manifest themselves as thermal inhomogeneities. Inhomogeneities in density, when large enough, are able to

Table 13. Total abundances compared

| | This work | | Liu et al. (2001) | | Ratag et al. (1997) |
|----|---------------------------------------|----------------|-------------------|-------|---------------------|
| | CEL | ORL | CEL | ORL | CEL |
| He | | 11.112 ± 0.008 | | 11.13 | 11.09 |
| C | | 9.36 ± 0.10 | 8.73 | 9.41 | |
| N | 8.95 ± 0.06 | 9.17 ± 0.11 | 8.42 | 9.17 | 8.62 |
| O | 8.79 ± 0.03 | 9.64 ± 0.04 | 8.85 | 9.64 | 8.89 |
| Ne | 8.36 ± 0.05 | 9.02 ± 0.07 | 8.57 | 9.16 | 8.27 |
| S | 7.35 ± _{0.12} ^{0.2} | | 7.47 | | 7.17 |
| Cl | 5.41 ± 0.08 | | 5.42 | | 5.98 |
| Ar | 6.77 ± 0.7 | | 6.66 | | 6.61 |
| Kr | 3.44 ± 0.15 | | | | |
| Xe | 2.83: | | | | |

Table 14. Abundance Discrepancy Factors. C⁺⁺ and N⁺⁺ ADFs were computed from our ORL abundances and the CEL abundances by Liu et al. (2001)

| Ion | ADF |
|----------------------------------|-------------|
| C ⁺⁺ /H ⁺ | 5.09 |
| N ⁺⁺ /H ⁺ | 7.30 |
| O ⁺⁺ /H ⁺ | 6.76 ± 0.50 |
| Ne ⁺⁺ /H ⁺ | 5.01 ± 0.52 |

distort our measurements by distorting nebular lines, which in turn affect the cooling and produce thermal inhomogeneities; also the expected chemical inhomogeneities will affect the number of coolants in the gas, producing thermal inhomogeneities (and probably inducing density inhomogeneities).

An empirical way to tackle the thermal inhomogeneities is the t^2 formalism developed by Peimbert (1967). But the only way to study chemical and density inhomogeneities is to include different phases in photoionization models (a modified version of this strategy can also be used to study thermal inhomogeneities).

6.1 Thermal inhomogeneities

The first evidence of a temperature structure in photoionized regions was reported by Peimbert (1967) who found a considerable difference between T_e derived from the Balmer Jump, and from forbidden line ratio diagnostics in the Orion Nebula. These differences are also found in PNe (see, for example Zhang et al. 2004). This led to the development of the t^2 formalism to account for temperature variations, further developed in Peimbert & Costero (1969).

To a second order approximation, the temperature structure of a photoionized region along the line of sight, can be characterized by the average temperature, T_0 , and the normalized mean square temperature fluctuation, t^2 , given by

$$T_0(X^{+i}) = \frac{\int T_e n_e n(X^{+i}) dV}{\int n_e n(X^{+i}) dV}, \quad (4)$$

and

$$t^2(X^{+i}) = \frac{\int (T_e - T_0(X^{+i}))^2 dV}{T_0(X^{+i})^2 \int n_e n(X^{+i}) dV}, \quad (5)$$

where n_e is the electron density and $n(X^{+i})$ is the density of ion X^{+i} . Note that while t^2 represents the mean square deviations, there is no definition for the rms deviations, and thus $\sqrt{t^2} \neq t$.

Table 15. t^2 derived from different methods

| Method | $t^2(\text{O II})$ | $t^2(\text{BJ})$ | $t^2(\text{He}^+)$ |
|--------|--------------------|------------------|--------------------|
| Value | 0.088 ± 0.003 | 0.048 ± 0.010 | 0.017 ± 0.003 |

To determine t^2 , two independent determinations of T_e are required; preferably comparing a temperature that uses lines that favor the hottest parts of a nebula with one that uses lines that favor the cooler parts of the nebula; temperatures derived using optical CELs will better represent the hotter parts, while those derived using ORLs will represent the cooler parts. In this work, besides the temperature determination from forbidden line ratios, we have used the Balmer Jump; T_e derived from helium ORLs, $T_e(\text{He I})$; and a hybrid O temperature equivalent to the ADF(O⁺⁺). Our results for t^2 are summarized in Table 15.

It must be noted that the three t^2 values obtained in Table 15 are irreconcilable. In other works, the t^2 values obtained from He I lines have been found to agree with those obtained from the Balmer Jump, $t^2(\text{BJ})$, and from the ADF(O⁺⁺), $t^2(\text{O II})$. Peimbert et al. (2014), for example find agreement in $t^2(\text{O}^{++})$ and $t^2(\text{He}^+)$ in part of a sample of low ADF PNe; however this is not the case for M 2-36. When these three values agree we are led to consider a single component with homogeneous chemical composition and density, but an internal temperature inhomogeneity; the fact that in M 2-36 they don't agree has led us to consider the possibility that the different gas phases in M 2-36 may not be well mixed, arising the question of which t^2 is more representative of the photoionized region in a global scale, if any.

6.2 Chemical inhomogeneities

In the last twenty years, observational evidence for the presence of chemical inhomogeneities has emerged. Notably, images of PN Abell 30 show clumps with ADFs exceeding 700 (Wesson et al. 2003), while the overall ADF of the object is around 70. Direct images of PNe have shown that emission from ORLs and CELs do not come from the same volume of gas (García-Rojas et al. 2016).

As mentioned before, chemical inhomogeneities will produce temperature fluctuations, which can be modeled using the t^2 formalism. From a mathematical point of view however, the t^2 is limited to relatively small temperature fluctuations. Chemical inhomogeneities are necessary to reproduce large ADF values observed in photoionized regions.

The usual approach when modeling chemical inhomogeneities in 1D consists of incorporating several phases with different chemistry.

Most commonly two-phase (bi-abundance) models are considered (see Tsamis & Péquignot 2005; Yuan et al. 2011, for example).

Typically, two-phase models include a phase with "normal" chemical composition; and another one with high density, including either high metallicity or poor hydrogen content (the difference between both scenarios being the treatment of He; also high metallicity inclusions are usually helium poor).

The implication of having a phase with very high density is that its mass becomes minimal, thus putting more weight on the hot phase, having a greater impact on the global chemistry of the object.

Consequently, chemical inhomogeneities can be adapted to produce any ADF value.

In the following section, we will show how a chemically inhomogeneous model reproduces important parameters reasonably.

7 A SIMPLE THREE-PHASE MODEL

The differences between $T_e(4363/4959)$, $T_e(V1/4959)$, $T_e(\text{BJ})$ and $T_e(\text{He}^+)$, are not consistent with a single phase model (not even one with an extreme t^2); in fact the wide dispersion of t^2 values present in Table 15, shows that these observations are not consistent with a chemically homogeneous PN. This in turn has led us to explore the possibility that more than one zone, each with radically different physical conditions, may coexist in the observed volume of PN M 2-36.

We have created "simple" two- and three-phase models using the photoionization code Cloudy V.17 (Ferland et al. 2017); the Py-Cloudy library (Morisset 2013) was also employed to write the Cloudy input files and define the weight of the gas phases.

The phases are distinguished mainly by their density and chemical composition (see Table 17). In the two phase models we used a low-metallicity low-density phase (Phase A), and a high metallicity phase; we explored the possibility of this second phase having a low to intermediate density, $10^3 \leq n_e \leq 10^4 \text{ cm}^{-3}$ (we call this Phase B), or high density, $n_e \sim 10^5 \text{ cm}^{-3}$ (we call this Phase C). For the three-phase models we included all three phases. The filling factor for each phase was also included as a variable in the model.

Initially we considered a black body as an ionizing source, however, while we had some success reproducing the observed forbidden line ratios, many line intensities were unsatisfactory; notably, He II $\lambda 4686$ was heavily overestimated. This led us to consider the PN atmosphere SEDs developed by Rauch (2003) with solar metallicity.

We find that a central star temperature (T_{eff}) of 80000 – 90000 K is consistent with our observations (Gurzadian 1988), hence we based our models around this interval. Since the conditions of the central star of M 2-36 are not well known, we sought a T_{eff} value able to reproduce reasonably the observed intensities of He II $\lambda 4686$ and C II $\lambda 4267$.

The final characteristic that is phase dependent is the relevance of each phase, which we weigh by a fraction of the total volume. Varying the weight of all three phases allows for too many degrees of freedom. Other characteristics of the model, such as radius, distance to the object, and the ratio of heavy elements to oxygen are the same for all phases. The corresponding values are included in Table 16.

Our approach to construct a grid of models was as follows. Abundances were set based on the observational results and modified in steps of 0.1 dex. The density of each phase and the external radius were set so that hydrogen was fully ionized in all phases. Large changes in $\log g$ mostly affected He II $\lambda 4686$ negatively, hence it was set to 5.0 (using a larger value would require us to increase T_{eff} above 90000 K). The best models were selected and refined in terms of line

intensities and ratios, comparing these with the observational results. Different weights for each phase were explored in every iteration.

Overall we constructed three sets of models, one with phases A and B; one with phases A and C; and the last one with all three phases. The best model from each set is presented in tables 17 (inputs) and 18 (outputs). Model 1 represents the best two-phased model that includes phases A and B, Model 2 represents the best two-phased model that includes phases A and C, and Model 3 represents the best three-phased model (we do not search for two phased models with phases B and C, because such high metallicities will never be able to reproduce the observed CEL ratios). In order to have a meaningful ADF we need to combine phase A with phase B and/or phase C.

We selected our preferred models by trying to fit simultaneously the traditional forbidden line intensity ratios (those used to determine temperature and density), as well as the fraction of O II V1 attributed to O II $\lambda 4649$ (an ORL density indicator; Peimbert & Peimbert 2013). The upper limit for this fraction is 0.40, which represents a global n_e in excess of 10^5 cm^{-3} , therefore we favored models that stay close to the observed value of 0.29, implying a density of 1100 cm^{-3} .

We present the fractional contributions from each phase to our three preferred models in Figure 6. Overall we can see that no phase dominates emission in any of the models.

In all models, Phase A is more evident in [O III] CELs and He II $\lambda 4686$, with a small contribution to the He I recombination lines, but being barely present in the heavy element recombination lines. High metallicity phases (either B, C, or both) dominate ORL emission in both two and three-phase models.

We chose to include the O II $\lambda 4649/V1$ ratio, since it is one of a very small set of line diagnostics that focuses on the cold/high metallicity gas. That being said, none of the two-phase models is able to simultaneously reproduce [O III] $\lambda 4959/\lambda 4363$ and O II $\lambda 4649/V1$ ratios (while reproducing the observed contrasts between CELs and ORLs). Model 1 reproduces the total intensity of O II V1 successfully and the $\lambda 4649/V1$ ratio acceptably, but fails to reproduce the CEL emission and ratios. The overall [O III] $\lambda 4959/\lambda 4363$ remains too low (too hot). In Model 2, the very high density of phase C lowers the cooling efficiency of the heavy elements allowing for moderate temperatures. However, the fraction of $4649/V1$ reaches an extreme value that is irreconcilable with our observations implying a total density of $\sim 10^5 \text{ cm}^{-3}$. After running hundreds of two-phase models, these trends were unavoidable. A combination of phases B and C is necessary to reproduce the O II $\lambda 4649/V1$ ratio in the high metallicity gas required by the observed ADF.

The idea of two-phased models has been proposed before to explain the abundances observed in some PNe and H II regions (Liu et al. 2000; Tsamis & Péquignot 2005; Yuan et al. 2011; Danehkar 2018), and has been expanded recently by Gómez-Llanos & Morisset (2020) (who constructed a bi-abundance, four-phased model for NGC 6153). Most of the two phased models in the literature include phases equivalent to our phases A and C, i.e. are equivalent to model 2; nonetheless we consider that it is important to try to place some constraints specific to the cold high metallicity gas, as we always do when working with the hot, low metallicity gas (such as the O II $\lambda 4649/V1$ ratio). When such additional constraints are included the results from models 1 and 2 fall short of being satisfactory, and force us into using more than two phases when modeling M 2-36.

We ran hundreds of three-phase models searching for a better fit. The best three-phase models are much better suited to reproduce our constraints than the best two-phase models. We are now able to reproduce the observed [O III] $\lambda 4959/\lambda 4363$ ratio, the O II V1 emissivity and an important departure from equilibrium of the $\lambda 4649/V1$ ratio. Overall we are also satisfied with individual emission lines, and

the other ratios presented in Table 18. We simultaneously reproduce some of the brightest emission lines with a maximum deviation of 22%. Still, a finer grid of models around these values is necessary to obtain better fits.

In the presence of chemical inhomogeneities the abundances present in any phase (or element of volume) are not representative of the entire object; neither CEL abundances nor ORL abundances are truly representative of the object as a whole. Gómez-Llanos & Morisset (2020) argue that the Abundance Contrast Factor (ACF), defined as the ratio of metal-rich to "normal" components in photoionization models is a better value for determining the true abundance difference than the ADF. In Models 1, 2, and 3, the logarithmic value of ACF(O) is 1.3, 1.63 and 1.63 respectively, implying that ADF(O⁺⁺) from our models is overestimated. Indeed, ADF(O⁺⁺) obtained from our model outputs is 4.98, 6.66 and 10.16. Taking their work as reference, a more realistic ADF(O⁺⁺) would be around 1.5 for all three models.

Observationally it is very difficult to properly characterize each of the phases (or even to determine the number of phases present in an object), and thus it is difficult to assess the global quantity of any element. On the other hand, when constructing a model we can have specific quantities of set phases built-in and thus have complete knowledge of the total quantities for all elements; in other words, we can "count" the atoms present in each phase and add them up. It must be emphasized that these abundances can not be measured directly from either real or synthetic spectra.

The total He/H and O/H abundances included in each model can be seen in Table 19. In all cases the abundances of the models are somewhat intermediate between those from the low metallicity and high metallicity phases. The O/H abundances are also intermediate between the observed CEL and ORL abundances; the exact value strongly depends on the mass of each phase, since the emission measure is somewhat similar for all phases, the lower the density of any given phase, the more relevant the chemical abundance of said phase is to the total object.

The high metallicity phases of our models have higher abundances than those determined from ORL (about 15% for He and a about factor of 2 to 4 for O). This arises because there is a significant contribution to the H lines from the low metallicity phase, thus diluting the O/H abundance seeded in the high metallicity phases.

In our interpretation of these three phases: phase C represents high-density, high-metallicity, low-volume inclusions which are probably being evaporated and thus are surrounded by a low-density, high-metallicity, high-volume medium (phase B); all these are immersed in a low-density, low-metallicity, high-volume "normal" medium (phase A). An interesting question is whether phase C represents nodules, filaments, or shells. This model does not really discriminate between those options, any of them can be represented by model 3.

As a last note on photoionization models, we would be remiss not to mention the possibility of the existence of more than 3 phases, or more accurately, more than 3 phases with a significant contribution to the overall line emission. While it is indeed possible, current observations do not give us enough constraints to discern the unique characteristics of so many phases, and a photoionization model, even a toy model, has too many degrees of freedom and thus the parameter space to study becomes too large to properly explore. Altogether it is beyond the scope of this paper to try to explore any such model.

Table 16. Input parameters of the best-fit models

| Parameter | Value |
|-----------------------|---------------------|
| Ionization Source | PN SED (Rauch 2003) |
| log <i>g</i> (source) | 5.0 |
| Distance (pc) | 6100 ^a |
| Ext. Radius (cm) | 10 ^{18.14} |
| log(C/O) | -0.53 |
| log(N/O) | -1.38 |
| log(Ne/O) | -0.98 |
| log(S/O) | -3.24 |
| log(Cl/O) | -3.1 |
| log(Ar/O) | -2.27 |

^a Stanghellini et al. (2008)

8 SUMMARY AND CONCLUSIONS

We have analyzed a high resolution spectrum of the planetary nebula M 2-36 obtained with the Ultraviolet and Visual Echelle Spectrograph at the Very Large Telescope covering the spectral range 3030–10360 Å. We measure the intensities of 420 emission features and, once blends are considered, we identify 446 emission lines. Notably, we identify three emission features from ions produced by the s-process ([Kr iv] λ5346 and λ5868; and [Xe iv] λ7536) marking the first detection of said elements in this nebula. Consequently we compute the total abundance of Kr and Xe.

We have computed T_e and n_e using traditional plasma diagnostics (from CELs). Our results are mostly consistent with a previous analysis of this object by Liu et al. (2001). We also computed T_e and n_e from ORLs of He⁺ and O⁺⁺ as well as from the Balmer jump (H⁺). All our CEL determinations are consistent with each other within a two zone photoionization scheme; this is particularly significant for the temperatures, due to the small error bars of our determinations.

Chemical abundances are reported for a large sample of ions. We have computed ionic abundances for C⁺⁺, N⁺⁺, O⁺⁺, and Ne⁺⁺ from ORLs and have obtained the corresponding ADFs. Given the quality of our spectrum, we produce a robust result for ADF(O⁺⁺) = 6.76 ± 0.50, this value is slightly larger than the one measured by Liu et al. (2001), but a difference is to be expected, since we are not observing the whole nebula (i.e. we do not observe the exact same volume).

The large value of ADF(O⁺⁺) cannot be attributed solely to the presence of temperature variations in a chemically homogeneous PN, thus suggesting the presence of at least two volumes of gas with different chemical composition.

Using the t^2 formalism of Peimbert (1967) we are able to determine three independent measurements for temperature inhomogeneities: $t^2(\text{O}^{++})$, $t^2(\text{He}^+)$ and $t^2(\text{H}^+)$. These determinations are not reconcilable under the assumption of chemical homogeneity; in fact the disparity between these three values reveals a complicated structure within the nebula and suggests the presence of more than two phases within the PN.

Our t^2 determinations motivated us to search for a simple photoionization model able to reproduce the general characteristics of M 2-36. We explored the possibility that a chemically inhomogeneous two-phased model was able to reproduce the observed characteristics of M 2-36, but were generally underwhelmed by the results. This setback, and previous suggestions to the existence of more than two phases, led us to explore the possibility that chemically inhomogeneous three-phase Cloudy models were better able to reproduce the observed emission of M 2-36.

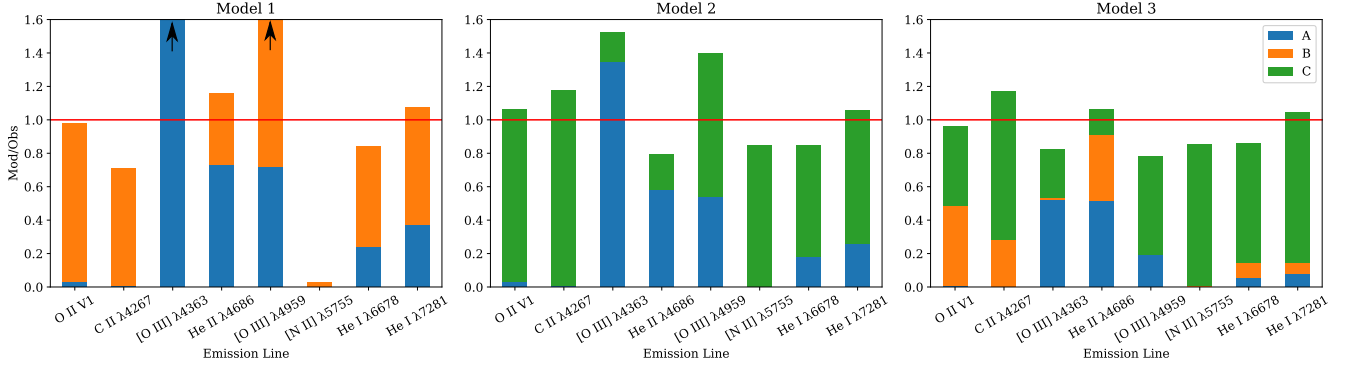


Figure 6. Comparison between model output and observations. Also shown is the contribution of each phase to line intensities.

Table 17. Parameters of the best-fit models.

| Phase | Two Phase Models | | | | Three Phase Model | | |
|------------------------------|------------------|---------------|---------------|---------------|-------------------|---------------|---------------|
| | 1 | | 2 | | 3 | | |
| | A | B | A | C | A | B | C |
| T_{eff} (K) | 90000 | | 82000 | | 84000 | | |
| $Q(H^0)$ | $10^{48.6}$ | | $10^{48.9}$ | | $10^{48.8}$ | | |
| Density (cm^{-3}) | 10^3 | 10^4 | $10^{2.9}$ | 10^5 | $10^{2.7}$ | $10^{3.0}$ | $10^{5.3}$ |
| Filling factor | 0.3 | 0.005 | 0.3 | 0.00005 | 0.25 | 0.011 | 0.00001 |
| Weight (Emis. measure) | $\frac{3}{5}$ | $\frac{2}{5}$ | $\frac{3}{5}$ | $\frac{2}{5}$ | $\frac{1}{3}$ | $\frac{1}{3}$ | $\frac{1}{3}$ |
| $\log(\text{He}/\text{H})$ | -0.880 | -0.834 | -0.880 | -0.834 | -0.880 | -0.834 | -0.834 |
| $\log(\text{O}/\text{H})$ | -3.35 | -2.05 | -3.35 | -1.72 | -3.35 | -1.72 | -1.72 |

Table 18. Line intensities outputs of the best-fit models.

| Emiss. line | $I(\lambda)/I(H\beta)$ | | | | | | |
|--|------------------------|---------|-------|---------|------|---------|------|
| | Obs. | Model 1 | | Model 2 | | Model 3 | |
| | | Mod | M/O | Mod | M/O | Mod | M/O |
| O II V1 sum. | 4.84 | 4.73 | 0.98 | 5.14 | 1.06 | 4.63 | 0.96 |
| [O II] $\lambda\lambda 3726+29$ | 1.84 | 90.85 | 49.38 | 2.55 | 1.38 | 2.61 | 1.42 |
| C II $\lambda 4267$ | 2.34 | 1.67 | 0.71 | 2.76 | 1.18 | 2.74 | 1.17 |
| [O III] $\lambda 4363$ | 2.8 | 5.54 | 1.98 | 4.26 | 1.52 | 2.28 | 0.81 |
| He II $\lambda 4686$ | 4.122 | 4.78 | 1.16 | 3.27 | 0.79 | 4.37 | 1.06 |
| [O III] $\lambda 4959$ | 263.64 | 458.79 | 1.74 | 367.82 | 1.40 | 206.43 | 0.78 |
| [N II] $\lambda 5755$ | 4.907 | 0.13 | 0.03 | 4.14 | 0.84 | 4.14 | 0.84 |
| He I $\lambda 6678$ | 5.88 | 4.96 | 0.84 | 5.01 | 0.85 | 5.07 | 0.86 |
| He I $\lambda 7281$ | 0.86 | 0.92 | 1.07 | 0.91 | 1.06 | 0.9 | 1.05 |
| Parameter | | | | | | | |
| O II $\lambda 4649/V1$ | 0.29 | 0.36 | 1.24 | 0.38 | 1.31 | 0.33 | 1.14 |
| [O III] $\lambda 4959/\lambda 4363$ | 90.90 | 85.10 | 0.94 | 85.10 | 0.94 | 90.73 | 0.99 |
| [N II] $\lambda 6548+\lambda 6584/\lambda 5755$ | 38.46 | 395.15 | 10.27 | 90.91 | 2.36 | 52.83 | 1.37 |
| [O III] $\lambda 4959/[O II] \lambda\lambda 3726+29$ | 4.16 | 5.05 | 1.20 | 3.29 | 0.78 | 2.60 | 0.63 |

Table 19. Chemical abundances from photoionization models

| Ratio | Obs | | Models | | |
|----------------------------|-------|--------|--------|--------|--------|
| | CEL | ORL | M1 | M2 | M3 |
| $\log(\text{He}/\text{H})$ | | -0.888 | -0.879 | -0.879 | -0.879 |
| $\log(\text{O}/\text{H})$ | -3.26 | -2.36 | -2.89 | -3.15 | -2.66 |

Our favorite model is able to reproduce the most relevant observed quantities related to O^{++} within an acceptable range, notably the nebular to auroral line ratio, the total intensity of multiplet V1, and the ratio of the intensity of multiplet V1 of $O\ II$ to $I(O\ II\ \lambda 4649)$, as well as to reproduce the observed He^+ and He^{++} line intensities.

While we are well pleased with the way our model fits the observations, this does not mean that M 2-36 is only composed by large quantities of matter that can be aligned with these three phases. First, it is very likely that there are better three-phase models than the one we found; second, there could be an important fraction of the emission of M 2-36 that comes from matter that corresponds to additional phases.

We must remark that the models presented in section 7 are only toy models. Our exploration has clear limitations: the grid we used could be refined, we do not explore in depth the abundances of other elements, it does not fully explore the effect of the mixing of three phases (it is the sum of three 1-D simulations), etc.

Our models show that, for M 2-36, the high metallicity gas must have at least some phase with low density (similar to that of the low metallicity gas). This means that there is a significant mass in the high metallicity gas, that must be taken into account when calculating the total abundances, and that the CEL abundances are not representative of the whole object (the fact that model 2 doesn't work means that we can not use the ORL abundances either). In fact our models show that the total abundances of M 2-36 are intermediate between CEL and ORL abundances.

Unfortunately our search for the best fit also showed us that the precise determination of total abundances depends strongly on the ratios between the emission measure of phases B and C and of the exact density of phase B.

The complexity of fitting a three phase model with only one set of observations limits the relevance of the abundance determinations of any such model. However, in this case, the exact O/H abundance appears to be close to the average between the CEL and ORL determinations.

While our tolerances do not permit us to explore the possibility of finding a model with more than three phases that produces a significantly better fit to the observed line intensities, we must ask ourselves whether such model exists. Furthermore, would more than three phases be required to model the gas component if we had deeper observations?. More importantly, is this model adequate to represent the real physical conditions within M 2-36?. Answers to those questions are beyond the scope of this paper.

Despite having been studied previously, our deep spectral analysis allowed us to discover that the chemistry of M 2-36 may be more complicated than previously thought. Our observations allowed us to measure critical quantities that characterize the object revealing the presence of at least three phases in the gas. This was possible largely thanks to the availability of temperature diagnostics from ORLs, whose use is not widespread and which are not always available.

This highlights the necessity of analyzing more objects similar to M 2-36 (with high but not extreme ADF) using a similar methodology. Since we do not expect all other high-ADF PNe to behave in the same way, we propose that many other high ADF objects should be studied specifically looking for evidence of both: low-density and high-density in their high metallicity components, before arriving to any conclusion regarding this type of objects.

In any case, it is clear that when determining the total abundances for PNe where the $O\ II\ \lambda 4649/VI$ ratio is less than ~ 0.40 the high metallicity regions can not be pushed aside and must be mixed with the low metallicity regions (i.e. when $O\ II\ \lambda 4649/VI$ is not consistent

with 0.40 the CEL abundances should not automatically be considered the correct abundances).

Regarding PNe with low to moderate ADFs, they should have several deep spectral analyses (independent of those of high ADF PNe) before arriving to any conclusion regarding these kind of objects and not to automatically assume objects like M 2-36 or Abell 30 can be used as models for objects with low ADF.

ACKNOWLEDGEMENTS

We wish to thank María Teresa Ruiz and Manuel Peimbert for their invaluable help with the observations. We thank an anonymous referee for numerous comments and suggestions that helped us improve the paper. J. N. Espíritu acknowledges the support of CONACyT grant 464709 and UNAM DGAPA/PAPIIT IG 100319 and IN103820. We also thank Verónica Gómez Llanos for her help with Python and Py-Cloudy. The manuscript of this paper has been written in the Overleaf environment.

DATA AVAILABILITY

This paper includes data collected at the European Southern Observatory, Chile, programme ID 70.C-0008(A). The photoionization models presented in this paper are available under request to the authors.

REFERENCES

- Bautista M. A., Ahmed E. E., 2018, *ApJ*, **866**, 43
 Biémont E., Hansen J. E., 1986, *Phys. Scr.*, **33**, 117
 Biémont E., Hansen J. E., Quinet P., Zeippen C. J., 1995, *A&AS*, **111**, 333
 Butler K., Zeippen C. J., 1989, *A&A*, **208**, 337
 Cardelli J. A., Clayton G. C., Mathis J. S., 1989, *ApJ*, **345**, 245
 Corradi R. L. M., García-Rojas J., Jones D., Rodríguez-Gil P., 2015, *ApJ*, **803**, 99
 D'Odorico S., Cristiani S., Dekker H., Hill V., Kaufer A., Kim T., Primas F., 2000, in Bergeron J., ed., *Society of Photo-Optical Instrumentation Engineers (SPIE) Conference Series Vol. 4005, Discoveries and Research Prospects from 8- to 10-Meter-Class Telescopes*. pp 121–130, doi:10.1117/12.390133
 Danehkar A., 2018, *Publ. Astron. Soc. Australia*, **35**, e005
 Davey A. R., Storey P. J., Kisielius R., 2000, *A&AS*, **142**, 85
 Delgado-Inglada G., Morisset C., Stasińska G., 2014, *MNRAS*, **440**, 536
 Ellis D. G., Martinson I., 1984, *Phys. Scr.*, **30**, 255
 Escalante V., Morisset C., Georgiev L., 2012, *MNRAS*, **426**, 2318
 Fang X., Storey P. J., Liu X. W., 2011, *A&A*, **530**, A18
 Ferland G. J., et al., 2017, *Rev. Mex. Astron. Astrofis.*, **53**, 385
 Froese Fischer C., Tachiev G., 2004, *Atomic Data and Nuclear Data Tables*, **87**, 1
 Galavis M. E., Mendoza C., Zeippen C. J., 1995, *A&AS*, **111**, 347
 Galavis M. E., Mendoza C., Zeippen C. J., 1997, *A&AS*, **123**, 159
 García-Rojas J., Esteban C., 2007, *ApJ*, **670**, 457
 García-Rojas J., Corradi R. L. M., Monteiro H., Jones D., Rodríguez-Gil P., Cabrera-Lavers A., 2016, *ApJ*, **824**, L27
 García-Rojas J., Wesson R., Boffin H. M. J., Jones D., Corradi R. L. M., Esteban C., Rodríguez-Gil P., 2019, arXiv e-prints, p. arXiv:1904.06763
 Gómez-Llanos V., Morisset C., 2020, *MNRAS*, **497**, 3363
 Grandi S. A., 1976, *ApJ*, **206**, 658
 Gurzadian G. A., 1988, *Ap&SS*, **149**, 343
 Henry R. B. C., Kwitter K. B., Balick B., 2004, *AJ*, **127**, 2284
 Kaufman V., Sugar J., 1986, *Journal of Physical and Chemical Reference Data*, **15**, 321
 Kingsburgh R. L., Barlow M. J., 1994, *MNRAS*, **271**, 257

Table 20. Emission line list

| λ_0 | λ_{obs} | Ion | Identification | F | I | Error (%) | Notes |
|-------------|------------------------|---------|----------------------|--------|---------|-----------|-------|
| 3187.74 | 3188.20 | He I | 3 | 1.652 | 2.578 | 8 | |
| 3203.10 | 3203.57 | He II | 3 | 0.542 | 0.817 | 13 | |
| 3218.19 | 3218.64 | Ne II | 4D ₀ -4F | 0.177 | 0.265 | 23 | |
| 3244.00 | 3244.54 | O II | 4P-D[2] ₀ | 0.086 | 0.127 | 32 | |
| 3334.87 | 3335.31 | Ne II | 2 | 0.390 | 0.559 | 15 | |
| 3354.56 | 3355.01 | He II | 1S-1P ₀ | 73.889 | 105.194 | 2 | |
| 3367.05 | 3367.70 | Ne II | 12 | 0.106 | 0.150 | 29 | |
| 3444.02 | 3444.55 | He I | 3P ₀ -3S | 1.327 | 1.845 | 8 | ? |
| 3447.63 | 3448.08 | He I | 3P ₀ -3D | 0.132 | 0.183 | 26 | |
| 3487.72 | 3488.13 | He I | 3P ₀ -3D | 0.068 | 0.093 | 36 | |
| 3498.64 | 3499.09 | He I | 3P ₀ -3D | 0.093 | 0.128 | 31 | |
| 3512.51 | 3513.02 | He I | 3P ₀ -3D | 0.138 | 0.189 | 26 | |
| 3530.50 | 3530.97 | He I | 3P ₀ -3D | 0.139 | 0.190 | 26 | |
| 3554.42 | 3554.88 | He I | 3P ₀ -3D | 0.196 | 0.266 | 22 | |
| 3587.28 | 3587.79 | He I | 3P ₀ -3D | 0.295 | 0.399 | 18 | |
| 3613.64 | 3614.15 | He I | 3P ₀ -3D | 0.277 | 0.372 | 18 | |
| 3634.25 | 3634.75 | He I | 3P ₀ -3D | 0.434 | 0.582 | 14 | |
| 3656.56 | 3657.16 | H I | H37 | 0.143 | 0.190 | 25 | |
| 3657.27 | 3657.77 | H I | H36 | 0.143 | 0.190 | 25 | |
| 3657.92 | 3658.41 | H I | H35 | 0.138 | 0.184 | 26 | |
| 3658.64 | 3659.11 | H I | H34 | 0.156 | 0.208 | 24 | |
| 3659.42 | 3659.95 | H I | H33 | 0.153 | 0.203 | 24 | |
| 3660.28 | 3660.79 | H I | H32 | 0.174 | 0.232 | 23 | |
| 3661.22 | 3661.71 | H I | H31 | 0.205 | 0.273 | 21 | |
| 3662.26 | 3662.75 | H I | H30 | 0.229 | 0.305 | 20 | |
| 3663.40 | 3663.90 | H I | H29 | 0.230 | 0.306 | 20 | |
| 3664.68 | 3665.14 | H I | H28 | 0.280 | 0.373 | 18 | |
| 3666.10 | 3666.61 | H I | H27 | 0.299 | 0.398 | 17 | |
| 3667.68 | 3668.18 | H I | H26 | 0.299 | 0.398 | 17 | |
| 3669.46 | 3669.97 | H I | H25 | 0.322 | 0.428 | 17 | |
| 3671.48 | 3671.99 | H I | H 24 | 0.364 | 0.485 | 16 | |
| 3673.76 | 3674.28 | H I | H23 | 0.361 | 0.480 | 16 | |
| 3676.36 | 3676.36 | H I | H22 | 0.378 | 0.503 | 16 | |
| 3679.35 | 3679.87 | H I | H 21 | 0.432 | 0.574 | 14 | |
| 3682.81 | 3683.32 | H I | H20 | 0.516 | 0.685 | 13 | |
| 3686.83 | 3687.34 | H I | H19 | 0.598 | 0.794 | 12 | |
| 3691.55 | 3692.07 | H I | H 18 | 0.750 | 0.995 | 11 | |
| 3694.22 | 3694.73 | Ne II | V1 | 0.270 | 0.358 | 18 | |
| 3697.15 | 3697.66 | H I | H 17 | 0.841 | 1.115 | 10 | |
| 3702.62 | 3703.22 | He I | 1P ₀ -1D | 0.088 | 0.117 | 32 | |
| 3703.86 | 3704.36 | H I | H 16 | 0.947 | 1.254 | 10 | |
| 3705.02 | 3705.52 | He I | 3P ₀ -3D | 0.719 | 0.951 | 11 | |
| 3707.25 | 3707.76 | He I | 1P ₀ -1S | 0.081 | 0.107 | 33 | |
| 3709.62 | 3710.12 | Ne II | V1 | 0.069 | 0.091 | 36 | |
| 3711.97 | 3712.49 | H I | H 15 | 1.158 | 1.530 | 9 | |
| 3713.08 | 3713.54 | Ne II | V5 | 0.262 | 0.346 | 19 | |
| 3721.87 | 3722.38 | [S III] | 2F | 2.072 | 2.733 | 7 | |
| 3721.93 | | H I | H 14 | | | | |
| 3726.03 | 3726.57 | [O II] | 1F | 31.155 | 41.072 | 2 | |
| 3727.25 | 3727.80 | N II | 3P ₀ -3D | 0.325 | 0.429 | 17 | |
| 3728.82 | 3729.32 | [O II] | 1F | 16.938 | 22.319 | 3 | |
| 3734.37 | 3734.89 | H I | H13 | 1.771 | 2.332 | 7 | |
| 3750.15 | 3750.65 | H I | H12 | 2.370 | 3.111 | 6 | |
| 3754.69 | 3755.22 | O III | V2 | 0.151 | 0.199 | 24 | |
| 3757.24 | 3757.75 | O III | V2 | 0.049 | 0.065 | 28 | |
| 3759.87 | 3760.41 | O III | V2 | 0.337 | 0.442 | 11 | |
| 3762.47 | 3762.99 | O II | V31 | 0.039 | 0.052 | 32 | |
| 3766.26 | 3766.78 | Ne II | V1 | 0.060 | 0.078 | 26 | |
| 3770.63 | 3771.15 | H I | H11 | 2.704 | 3.536 | 4 | |
| 3774.02 | 3774.54 | O III | V2 | 0.047 | 0.062 | 29 | |
| 3777.14 | 3777.67 | Ne II | V1 | 0.071 | 0.093 | 24 | |
| 3784.89 | 3785.43 | He I | V64 | 0.033 | 0.042 | 35 | |
| 3791.27 | 3791.84 | O III | V2 | 0.051 | 0.066 | 28 | |

Table 20 – *continued*

| λ_0 | λ_{obs} | Ion | Identification | F | I | Error (%) | Notes |
|-------------|------------------------|----------|---------------------|--------|--------|-----------|-------|
| 3797.90 | 3798.43 | H I | H10 | 3.658 | 4.759 | 4 | |
| 3805.74 | 3806.31 | He I | V63 | 0.070 | 0.091 | 24 | |
| 3806.49 | 3807.01 | Si III | V5 | 0.041 | 0.054 | 31 | |
| 3819.61 | 3820.17 | He I | V22 | 1.261 | 1.634 | 6 | |
| 3829.77 | 3830.25 | Ne II | V39 | 0.037 | 0.048 | 33 | |
| 3833.55 | 3834.08 | He I | V62 | 0.066 | 0.086 | 24 | |
| 3835.39 | 3835.92 | H I | H 9 | 5.409 | 6.986 | 3 | |
| 3856.02 | 3856.58 | Si II | V1 | 0.115 | 0.147 | 19 | |
| 3862.59 | 3863.14 | Si II | V1 | 0.135 | 0.174 | 17 | |
| 3868.75 | 3869.30 | [Ne III] | F1 | 62.759 | 80.525 | 2 | |
| 3871.79 | 3872.32 | He I | 1P ₀ -1D | 0.084 | 0.108 | 22 | |
| 3880.33 | 3880.80 | Ar II | 54 | 0.046 | 0.059 | 29 | |
| 3882.19 | 3882.76 | O II | V12 | 0.116 | 0.149 | 18 | |
| 3888.65 | 3889.42 | He I | V2 | 16.892 | 21.584 | 2 | |
| 3889.05 | | H I | H8 | | | | |
| 3912.72 | 3913.32 | Mn I | | 0.037 | 0.047 | 33 | ? |
| 3920.59 | 3921.18 | C II | V4 | 0.040 | 0.051 | 31 | |
| 3926.53 | 3927.11 | He I | V58 | 0.125 | 0.159 | 18 | |
| 3964.74 | 3965.28 | He I | V5 | 0.891 | 1.120 | 7 | |
| 3967.46 | 3967.98 | [Ne III] | 1F | 11.000 | 13.819 | 2 | |
| 3968.43 | | He I | 4.14 | | | | |
| 3970.07 | 3970.63 | H I | H7 | 15.857 | 19.910 | 2 | |
| 3973.24 | 3973.81 | O II | 6 | 0.103 | 0.130 | 20 | |
| 3979.78 | 3980.29 | [Fe II] | F9 | 0.049 | 0.061 | 28 | |
| 3979.93 | | [Fe II] | F8 | | | | |
| 3994.99 | 3995.54 | N II | V12 | 0.050 | 0.063 | 28 | |
| 4009.26 | 4009.82 | He I | V55 | 0.269 | 0.335 | 12 | |
| 4013.99 | 4014.59 | Ne I | 2 | 0.033 | 0.041 | 35 | |
| 4023.98 | 4024.51 | He I | 1P ₀ -1S | 0.032 | 0.040 | 35 | |
| 4026.21 | 4026.76 | He I | V18 | 4.649 | 5.762 | 3 | |
| 4035.07 | 4035.65 | O II | V68 | 0.113 | 0.139 | 19 | |
| 4035.08 | | N II | V39a | | | | |
| 4041.31 | 4041.88 | N II | V39 | 0.201 | 0.248 | 14 | |
| 4043.53 | 4044.08 | N II | V39 | 0.074 | 0.091 | 23 | |
| 4062.94 | 4063.51 | O II | V50 | 0.131 | 0.161 | 17 | |
| 4068.60 | 4069.14 | [S II] | 1F | 4.339 | 5.323 | 3 | |
| 4069.62 | 4070.38 | O II | V10 | 1.412 | 1.732 | 5 | |
| 4069.89 | | O II | V10 | | | | |
| 4071.24 | 4071.80 | O II | V48a | 0.084 | 0.103 | 22 | |
| 4072.15 | 4072.73 | O II | V10 | 0.894 | 1.096 | 7 | |
| 4075.86 | 4076.51 | O II | V10 | 1.368 | 1.676 | 6 | |
| 4076.56 | 4077.12 | S II | F1 | 0.519 | 0.635 | 9 | |
| 4078.84 | 4079.41 | O II | V10 | 0.117 | 0.144 | 18 | |
| 4083.89 | 4084.46 | O II | V48b | 0.123 | 0.151 | 18 | |
| 4085.11 | 4085.68 | O II | V10 | 0.146 | 0.178 | 16 | |
| 4087.15 | 4087.72 | O II | V48 | 0.143 | 0.174 | 17 | |
| 4089.29 | 4089.84 | O II | V48 | 0.469 | 0.572 | 9 | |
| 4092.93 | 4093.50 | O II | V10 | 0.110 | 0.135 | 19 | |
| 4095.66 | 4096.23 | O II | V48 | 0.113 | 0.138 | 19 | |
| 4097.32 | 4097.88 | O II | V48 | 1.856 | 2.261 | 5 | |
| 4098.24 | 4098.79 | O II | V46a | 0.110 | 0.134 | 19 | |
| 4100.05 | 4100.62 | He II | V4 | 0.113 | 0.138 | 19 | |
| 4101.75 | 4102.32 | H I | H 6 | 33.631 | 40.926 | 2 | |
| 4103.39 | 4103.95 | N III | V1 | 1.010 | 1.229 | 6 | |
| 4104.95 | 4105.51 | O II | V20 | 0.192 | 0.233 | 14 | |
| 4107.10 | 4107.67 | O II | V48 | 0.098 | 0.119 | 20 | |
| 4110.79 | 4111.37 | O II | V20 | 0.094 | 0.115 | 20 | |
| 4119.22 | 4119.79 | O II | V20 | 0.270 | 0.328 | 12 | |
| 4120.82 | 4121.31 | He I | V16 | 0.316 | 0.383 | 11 | |
| 4121.46 | 4122.07 | O II | V19 | 0.069 | 0.083 | 24 | |
| 4132.80 | 4133.37 | O II | V19 | 0.138 | 0.167 | 17 | |
| 4143.76 | 4144.33 | He I | V53 | 0.494 | 0.595 | 9 | |
| 4145.90 | 4146.66 | O II | V106 | 0.040 | 0.048 | 31 | |

Table 20 – continued

| λ_0 | λ_{obs} | Ion | Identification | F | I | Error (%) | Notes |
|-------------|------------------------|---------|------------------------|--------|--------|-----------|-------|
| 4146.08 | | O II | V106 | | | | |
| 4153.30 | 4153.87 | O II | V19 | 0.268 | 0.322 | 12 | |
| 4156.53 | 4156.96 | O II | V19 | 0.116 | 0.139 | 18 | |
| 4168.97 | 4169.73 | He I | V52 | 0.119 | 0.143 | 18 | |
| 4171.61 | 4172.20 | N II | V43a | 0.036 | 0.043 | 33 | |
| 4176.16 | 4176.71 | N II | V43a | 0.066 | 0.079 | 24 | |
| 4185.45 | 4186.01 | O II | V36 | 0.089 | 0.106 | 21 | |
| 4186.89 | 4187.47 | C III | V18 | 0.061 | 0.073 | 25 | |
| 4189.78 | 4190.36 | O II | V36 | 0.114 | 0.135 | 19 | |
| 4195.76 | 4196.33 | N III | V6 | 0.041 | 0.048 | 31 | |
| 4199.83 | 4200.56 | He II | 4.11 | 0.137 | 0.162 | 17 | |
| 4217.15 | 4217.73 | N II | 3Po – 3P | 0.034 | 0.040 | 34 | |
| 4219.76 | 4220.32 | Ne II | V52 | 0.097 | 0.115 | 20 | |
| 4231.53 | 4232.18 | Ne II | V52b | 0.039 | 0.046 | 32 | |
| 4236.91 | 4237.56 | N II | V48 | 0.106 | 0.125 | 19 | |
| 4237.05 | | N II | V48 | | | | |
| 4241.78 | 4242.38 | N II | V48 | 0.163 | 0.192 | 16 | |
| 4254.00 | 4254.61 | O II | 109 | 0.043 | 0.050 | 30 | |
| 4267.15 | 4267.76 | C II | V6 | 2.011 | 2.344 | 5 | |
| 4275.55 | 4276.16 | O II | V67 | 0.222 | 0.258 | 13 | |
| 4276.75 | 4277.26 | O II | V67 | 0.095 | 0.111 | 20 | |
| 4277.43 | 4278.02 | O II | V67c | 0.050 | 0.058 | 28 | |
| 4281.32 | 4281.92 | O II | 53b | 0.018 | 0.021 | 46 | |
| 4282.96 | 4283.58 | O II | 67c | 0.061 | 0.070 | 25 | |
| 4283.73 | 4284.32 | O II | V67c | 0.032 | 0.038 | 35 | |
| 4285.70 | 4286.29 | O II | V78b | 0.070 | 0.081 | 24 | |
| 4288.81 | 4289.40 | O II | V53c | 0.026 | 0.030 | 39 | |
| 4291.25 | 4291.86 | O II | V55 | 0.076 | 0.088 | 23 | |
| 4292.21 | 4292.85 | O II | V78c | 0.061 | 0.071 | 25 | |
| 4294.92 | 4295.40 | O II | V54 | 0.125 | 0.145 | 18 | |
| 4303.61 | 4304.40 | O II | V65a | 0.238 | 0.275 | 13 | |
| 4303.82 | | O II | V53a | | | | |
| 4307.23 | 4307.82 | O II | V54 | 0.044 | 0.051 | 30 | |
| 4309.02 | 4309.61 | O II | 4D – D[1] ₀ | 0.029 | 0.033 | 37 | |
| 4313.44 | 4314.03 | O II | V78a | 0.042 | 0.048 | 31 | |
| 4315.40 | 4316.00 | O II | V63c | 0.031 | 0.035 | 36 | |
| 4317.15 | 4317.74 | O II | V2 | 0.152 | 0.175 | 16 | |
| 4319.63 | 4320.22 | O II | V2 | 0.106 | 0.122 | 19 | |
| 4325.76 | 4326.36 | O II | V2 | 0.037 | 0.043 | 32 | |
| 4329.75 | 4330.37 | C II | 2D–Fo | 0.013 | 0.015 | 54 | |
| 4331.14 | 4331.74 | O II | V65b | 0.036 | 0.041 | 33 | |
| 4332.71 | 4333.32 | O II | 65 | 0.058 | 0.066 | 26 | |
| 4336.86 | 4337.46 | O II | V2 | 0.053 | 0.061 | 27 | |
| 4338.69 | 4339.29 | He II | 4–10 | 0.063 | 0.072 | 25 | |
| 4340.47 | 4341.07 | H I | H5 | 39.645 | 45.317 | 2 | |
| 4344.39 | 4344.99 | O I] | | 0.038 | 0.044 | 32 | ? |
| 4345.56 | 4346.16 | O II | V2 | 0.175 | 0.199 | 15 | |
| 4349.43 | 4350.03 | O II | V2 | 0.310 | 0.353 | 11 | |
| 4351.51 | 4352.11 | O II | V16 | 0.065 | 0.074 | 25 | |
| 4353.60 | 4354.20 | O II | V76c | 0.046 | 0.052 | 29 | |
| 4357.27 | 4357.87 | O II | V63a | 0.027 | 0.031 | 38 | |
| 4363.21 | 4363.81 | [O III] | 2F | 2.465 | 2.800 | 4 | |
| 4366.89 | 4367.47 | O II | V2 | 0.185 | 0.210 | 15 | |
| 4371.59 | 4372.21 | O II | V76b | 0.055 | 0.063 | 27 | |
| 4379.11 | 4379.76 | N III | V18b | 0.380 | 0.430 | 10 | |
| 4379.55 | | Ne III | V60b | | | | |
| 4387.93 | 4388.54 | He I | V51 | 0.694 | 0.783 | 8 | |
| 4391.94 | 4392.60 | Ne II | V55e | 0.118 | 0.133 | 18 | |
| 4397.98 | 4398.58 | Ne II | V57b | 0.027 | 0.031 | 38 | |
| 4409.30 | 4409.91 | Ne II | V55e | 0.094 | 0.106 | 20 | |
| 4413.11 | 4413.81 | Ne II | V57c | 0.036 | 0.041 | 33 | |
| 4413.11 | | Ne II | V65 | | | | |
| 4413.22 | | Ne II | V55 | | | | |

Table 20 – *continued*

| λ_0 | λ_{obs} | Ion | Identification | F | I | Error (%) | Notes |
|-------------|------------------------|----------|---------------------|-------|-------|-----------|-------|
| 4414.90 | 4415.51 | O II | V5 | 0.147 | 0.165 | 16 | |
| 4416.97 | 4417.59 | O II | V5 | 0.121 | 0.135 | 18 | |
| 4416.97 | | O II | V5 | | | | |
| 4428.54 | 4429.16 | Ne II | V57 | 0.065 | 0.073 | 25 | |
| 4430.94 | 4431.56 | Ne II | V61 | 0.042 | 0.047 | 30 | |
| 4432.74 | 4433.34 | N II | V55a | 0.076 | 0.085 | 23 | |
| 4434.60 | 4435.21 | O III | G[9/2]-H[11/2]o | 0.040 | 0.045 | 31 | |
| 4437.55 | 4438.16 | He I | 1P ₀ -1S | 0.065 | 0.072 | 25 | |
| 4439.46 | 4439.95 | Ar II | 2D ₀ -2D | 0.022 | 0.025 | 42 | |
| 4439.88 | | Ar II | 2D ₀ -2D | | | | |
| 4457.05 | 4457.70 | Ne II | V61a | 0.038 | 0.043 | 32 | |
| 4457.26 | | Ne II | V61d | | | | |
| 4466.43 | 4467.04 | O II | V86b | 0.044 | 0.049 | 30 | |
| 4469.45 | 4470.06 | O II | 4D – 4P | 0.032 | 0.035 | 35 | |
| 4471.47 | 4472.12 | He I | V14 | 6.251 | 6.897 | 3 | |
| 4477.90 | 4478.17 | O II | V88 | 0.115 | 0.127 | 19 | |
| 4481.21 | 4481.85 | Mg II | V4 | 0.039 | 0.042 | 32 | |
| 4489.45 | 4490.07 | O II | V86b | 0.022 | 0.024 | 43 | |
| 4491.23 | 4491.86 | O II | V86a | 0.097 | 0.107 | 20 | |
| 4498.92 | 4499.62 | Ne II | V64c | 0.025 | 0.028 | 39 | |
| 4499.12 | | Ne II | V64c | | | | |
| 4510.91 | 4511.53 | N III | V3 | 0.221 | 0.241 | 13 | |
| 4514.86 | 4515.48 | N III | V3 | 0.042 | 0.046 | 31 | |
| 4518.15 | 4518.75 | N III | V3 | 0.074 | 0.081 | 23 | |
| 4520.69 | 4521.34 | Si II | 2D-2P ₀ | 0.056 | 0.061 | 27 | |
| 4523.58 | 4524.22 | N III | V3 | 0.051 | 0.056 | 28 | |
| 4530.41 | 4531.04 | N II | V58b | 0.104 | 0.113 | 19 | |
| 4530.86 | | N III | V3 | | | | |
| 4534.58 | 4535.15 | N III | V3 | 0.037 | 0.040 | 33 | |
| 4541.59 | 4542.24 | He II | 4.9 | 0.074 | 0.080 | 23 | |
| 4544.85 | 4545.47 | N III | V12 | 0.020 | 0.022 | 44 | |
| 4552.52 | 4553.22 | N II | V58a | 0.068 | 0.074 | 24 | |
| 4562.60 | 4563.22 | Mg I] | | 0.072 | 0.078 | 23 | |
| 4571.10 | 4571.73 | Mg I] | | 0.499 | 0.536 | 9 | |
| 4590.97 | 4591.60 | O II | V15 | 0.116 | 0.124 | 18 | |
| 4595.95 | 4596.79 | O II | V15 | 0.086 | 0.092 | 21 | |
| 4596.18 | | O II | V15 | | | | |
| 4602.13 | 4602.69 | O II | V92b | 0.118 | 0.126 | 18 | |
| 4607.16 | 4607.81 | N II | V5 | 0.033 | 0.035 | 35 | |
| 4609.44 | 4610.07 | O II | V92a | 0.236 | 0.251 | 13 | |
| 4610.20 | 4610.87 | O II | V92c | 0.141 | 0.150 | 17 | |
| 4613.68 | 4614.43 | O II | V92b | 0.037 | 0.039 | 33 | |
| 4620.26 | 4621.08 | C II | | 0.057 | 0.060 | 26 | ? |
| 4621.39 | 4622.02 | N II | V5 | 0.056 | 0.060 | 26 | |
| 4630.54 | 4631.18 | N II | V5 | 0.281 | 0.298 | 12 | |
| 4634.14 | 4634.78 | N III | V2 | 1.301 | 1.375 | 6 | |
| 4638.86 | 4639.50 | O II | V1 | 0.645 | 0.681 | 8 | |
| 4640.64 | 4641.28 | N III | V2 | 1.820 | 1.920 | 5 | |
| 4641.83 | 4642.47 | O II | V1 | 1.302 | 1.373 | 6 | |
| 4643.06 | 4643.73 | N II | V5 | 0.047 | 0.050 | 29 | |
| 4647.45 | 4648.09 | C III | V1 | 0.108 | 0.113 | 19 | |
| 4649.13 | 4649.78 | O II | V1 | 1.353 | 1.424 | 6 | |
| 4650.84 | 4651.49 | O II | V1 | 0.404 | 0.425 | 10 | |
| 4656.39 | 4657.02 | Ne I | 3/2[1/2]-1/2[1/2]o | 0.077 | 0.081 | 23 | |
| 4658.05 | 4658.67 | [Fe III] | 3F | 0.057 | 0.060 | 26 | |
| 4661.63 | 4662.27 | O II | V1 | 0.479 | 0.503 | 9 | |
| 4669.27 | 4669.98 | O II | V89b | 0.023 | 0.024 | 42 | |
| 4673.73 | 4674.38 | O II | V1 | 0.063 | 0.066 | 25 | |
| 4676.24 | 4676.87 | O II | V1 | 0.307 | 0.321 | 11 | |
| 4678.11 | 4678.76 | N II | V61b | 0.019 | 0.020 | 45 | |
| 4685.71 | 4686.40 | He II | 4-3 | 3.952 | 4.122 | 3 | ? |
| 4694.66 | 4695.31 | N II | V61a | 0.032 | 0.033 | 35 | |
| 4696.35 | 4696.98 | O II | V1 | 0.051 | 0.053 | 28 | |

Table 20 – continued

| λ_0 | λ_{obs} | Ion | Identification | F | I | Error (%) | Notes |
|-------------|------------------------|----------|-------------------------|---------|---------|-----------|-----------|
| 4699.22 | 4699.83 | O II | V25 | 0.030 | 0.031 | 36 | |
| 4703.16 | 4704.02 | O II | 2D ₀ -2F | 0.055 | 0.057 | 27 | |
| 4703.36 | | Ar II | | | | | |
| 4705.35 | 4705.99 | O II | V25 | 0.039 | 0.040 | 32 | |
| 4710.00 | 4710.67 | O II | | 0.035 | 0.037 | 33 | |
| 4711.37 | 4712.03 | [Ar IV] | 1F | 1.291 | 1.338 | 6 | |
| 4713.17 | 4713.83 | He I | V12 | 0.690 | 0.714 | 8 | |
| 4740.23 | 4740.88 | [Ar IV] | 1F | 1.453 | 1.495 | 5 | |
| 4751.34 | 4752.02 | O II | | 0.075 | 0.077 | 23 | |
| 4762.31 | 4762.89 | C I | 6 | 0.027 | 0.028 | 38 | |
| 4788.13 | 4788.82 | N II | 20 | 0.020 | 0.021 | 44 | |
| 4802.23 | 4803.11 | C II | | 0.068 | 0.069 | 24 | |
| 4803.27 | 4803.93 | N II | V20 | 0.073 | 0.074 | 23 | |
| 4815.51 | 4816.20 | S II | 9 | 0.025 | 0.026 | 39 | |
| 4859.36 | 4860.03 | He II | 8-4 | 0.181 | 0.181 | 15 | |
| 4861.33 | 4862.00 | H I | H β | 100.000 | 99.986 | 2 | |
| 4890.86 | 4891.53 | O II | V28 | 0.028 | 0.028 | 37 | |
| 4901.28 | 4902.13 | S II | | 0.114 | 0.113 | 19 | |
| 4902.65 | 4903.32 | Si II | | 0.026 | 0.026 | 39 | |
| 4921.93 | 4922.62 | He I | V48 | 1.701 | 1.678 | 5 | |
| 4924.53 | 4925.20 | O II | V28 | 0.152 | 0.150 | 16 | |
| 4931.32 | 4931.91 | [O III] | F1 | 0.091 | 0.090 | 21 | |
| 4958.91 | 4959.63 | [O III] | 1 | 269.852 | 264.011 | 2 | |
| 5006.84 | 5007.56 | [O III] | F1 | 746.310 | 722.761 | 2 | Saturated |
| 5015.70 | 5016.39 | He I | V4 | 2.819 | 2.725 | 4 | |
| 5025.66 | 5026.32 | N II | 1V9 | 0.018 | 0.017 | 43 | |
| 5032.13 | 5032.94 | C II | 2P-2D | 0.039 | 0.038 | 29 | |
| 5041.12 | 5041.74 | Si II | V5 | 0.329 | 0.316 | 10 | |
| 5055.98 | 5056.86 | Si II | V5 | 0.131 | 0.125 | 16 | |
| 5121.82 | 5122.57 | C II | V12 | 0.048 | 0.045 | 26 | |
| 5191.82 | 5192.43 | [Ar III] | F3 | 0.055 | 0.052 | 24 | |
| 5197.90 | 5198.63 | [N I] | F1 | 0.715 | 0.667 | 7 | |
| 5200.06 | 5200.97 | [Fe II] | F19 | 0.512 | 0.478 | | |
| 5200.26 | | [N I] | F1 | | | 8 | |
| 5270.40 | 5271.19 | [Fe III] | F1 | 0.032 | 0.030 | 32 | |
| 5342.38 | 5343.15 | C II | 17.06 | 0.127 | 0.116 | 16 | |
| 5346.02 | 5346.62 | [Kr IV] | 1F | 0.019 | 0.017 | 42 | ? |
| 5405.15 | 5405.91 | Ne II | 2[5] ₀ -2[6] | 0.031 | 0.028 | 33 | |
| 5411.52 | 5412.30 | He II | 4.7 | 0.334 | 0.301 | 10 | |
| 5453.81 | 5454.67 | S II | V6 | 0.030 | 0.027 | 33 | |
| 5495.67 | 5496.45 | N II | V29 | 0.018 | 0.016 | 43 | |
| 5517.71 | 5518.45 | [Cl III] | F1 | 0.666 | 0.590 | 7 | |
| 5537.88 | 5538.62 | [Cl III] | F1 | 0.898 | 0.793 | 6 | |
| 5577.34 | 5578.46 | [O I] | F3 | 0.044 | 0.039 | 27 | |
| 5666.64 | 5667.41 | N II | V3 | 0.287 | 0.249 | 11 | |
| 5676.02 | 5676.80 | N II | V3 | 0.121 | 0.105 | 17 | |
| 5679.56 | 5680.35 | N II | V3 | 0.674 | 0.584 | 7 | |
| 5686.21 | 5687.01 | N II | V3 | 0.081 | 0.070 | 20 | |
| 5710.76 | 5711.54 | N II | V3 | 0.121 | 0.104 | 17 | |
| 5739.73 | 5740.61 | Si III | V4 | 0.018 | 0.016 | 43 | |
| 5747.33 | 5748.22 | O II | 2D ₀ -2F | 0.057 | 0.049 | 24 | |
| 5754.64 | 5755.43 | [N II] | 3F | 5.720 | 4.907 | 3 | |
| 5867.74 | 5868.56 | [Kr IV] | 4S-2D | 0.024 | 0.021 | 22 | |
| 5875.60 | 5876.48 | He I | V11 | 22.009 | 18.602 | 2 | |
| 5927.78 | 5928.59 | N II | V28 | 0.020 | 0.016 | 25 | |
| 5931.85 | 5932.72 | He II | 5.25 | 0.066 | 0.055 | 14 | ? |
| 5940.24 | 5941.07 | N II | V28 | 0.013 | 0.011 | 31 | |
| 5941.65 | 5942.46 | N II | V28 | 0.092 | 0.077 | 12 | |
| 5952.58 | 5953.40 | He II | 5.23 | 0.026 | 0.022 | 22 | ? |
| 5957.56 | 5958.24 | Si II | V4 | 0.010 | 0.008 | 36 | |
| 5978.98 | 5979.81 | Si II | V4 | 0.025 | 0.021 | 22 | |
| 6074.13 | 6074.97 | He II | 5.20 | 0.015 | 0.013 | 28 | |
| 6101.83 | 6102.62 | [K IV] | F1 | 0.090 | 0.074 | 12 | |

Table 20 – *continued*

| λ_0 | λ_{obs} | Ion | Identification | F | I | Error (%) | Notes |
|-------------|------------------------|----------|-------------------------|---------|---------|-----------|-------|
| 6151.43 | 6152.23 | C II | 16.04 | 0.087 | 0.072 | 12 | |
| 6157.42 | 6158.40 | Ni II | | 0.023 | 0.019 | 23 | ? |
| 6233.82 | 6234.43 | He II | 5.17 | 0.019 | 0.016 | 25 | |
| 6300.30 | 6301.19 | [O I] | F1 | 8.701 | 7.066 | 2 | |
| 6312.10 | 6312.97 | [S III] | 3F | 1.830 | 1.484 | 3 | |
| 6347.11 | 6348.01 | Si II | V2 | 0.158 | 0.126 | 9 | |
| 6363.78 | 6364.68 | [O I] | F1 | 2.944 | 2.375 | 3 | |
| 6371.36 | 6372.26 | Si II | V2 | 0.236 | 0.189 | 7 | |
| 6402.25 | 6403.10 | Ne I | V1 | 0.014 | 0.011 | 30 | ? |
| 6406.38 | 6407.24 | He II | 5-15 | 0.013 | 0.010 | 31 | |
| 6461.95 | 6462.75 | C II | 17.04 | 0.315 | 0.250 | 6 | |
| 6482.05 | 6482.96 | N II | V8 | 0.030 | 0.023 | 20 | |
| 6485.30 | 6485.907 | [Fe II] | b4P-a2S | 0.028 | 0.022 | 21 | |
| 6486.46 | 6487.33 | O II | G[3] ₀ -I[4] | 0.029 | 0.023 | 21 | |
| 6527.24 | 6528.053 | [N II] | F1 | 0.041 | 0.032 | 17 | |
| 6548.03 | 6549.003 | [N II] | F1 | 59.658 | 46.867 | 2 | |
| 6560.18 | 6561.08 | He II | 6-4 | 0.763 | 0.598 | 4 | |
| 6562.82 | 6563.72 | H I | H α | 379.784 | 297.894 | 2 | |
| 6578.05 | 6578.96 | C II | V2 | 0.896 | 0.701 | 4 | |
| 6583.41 | 6584.38 | [N II] | F1 | 185.048 | 144.835 | 2 | |
| 6678.15 | 6679.08 | He I | V46 | 7.528 | 5.834 | 2 | |
| 6683.27 | 6684.19 | Ne II | 2[2] ₀ -4D | 0.026 | 0.020 | 22 | |
| 6716.47 | 6717.40 | [S II] | F2 | 12.618 | 9.740 | 2 | |
| 6721.39 | 6722.28 | O II | V4 | 0.012 | 0.009 | 32 | |
| 6730.85 | 6731.79 | [S II] | F2 | 20.368 | 15.699 | 2 | |
| 6744.39 | 6745.21 | N II | 3.000 | 0.008 | 0.006 | 38 | |
| 6780.06 | 6780.97 | C II | V14 | 0.017 | 0.013 | 27 | |
| 6809.99 | 6811.11 | N II | V54 | 0.005 | 0.004 | 38 | |
| 6821.16 | 6822.31 | [Mn III] | | 0.008 | 0.006 | 32 | ? |
| 6933.89 | 6934.88 | He I | 1/13 | 0.014 | 0.011 | 26 | |
| 6989.47 | 6990.48 | He I | 1/12 | 0.021 | 0.016 | 22 | |
| 7062.26 | 7063.35 | He I | 1/11 | 0.037 | 0.028 | 16 | |
| 7065.28 | 7066.25 | He I | V10 | 9.924 | 7.458 | 2 | |
| 7135.78 | 7136.79 | [Ar III] | F1 | 32.270 | 24.076 | 2 | |
| 7160.61 | 7161.55 | He I | 1/10 | 0.055 | 0.041 | 14 | |
| 7231.34 | 7232.32 | C II | V3 | 0.660 | 0.487 | 4 | |
| 7236.42 | 7237.46 | C II | V3 | 1.529 | 1.129 | 3 | |
| 7262.76 | 7263.95 | [Ar IV] | F2 | 0.037 | 0.027 | 16 | |
| 7281.35 | 7282.39 | He I | V45 | 1.175 | 0.864 | 3 | |
| 7318.92 | 7320.95 | [O II] | F2 | 6.587 | 4.822 | 2 | |
| 7319.99 | | [O II] | F2 | | | | |
| 7329.66 | 7331.23 | [O II] | F2 | 5.367 | 3.925 | 2 | |
| 7330.73 | | [O II] | F2 | | | | |
| 7499.85 | 7500.85 | He I | 1/8 | 0.087 | 0.062 | 11 | |
| 7519.49 | 7520.78 | C II | 16.08 | 0.009 | 0.007 | 32 | |
| 7519.86 | | C II | 16.08 | | | | |
| 7530.54 | 7531.51 | [Cl IV] | F1 | 0.377 | 0.270 | 5 | |
| 7535.40 | 7536.07 | [Xe IV] | 4S-2D | 0.008 | 0.006 | 35 | |
| 7751.10 | 7752.19 | [Ar III] | F2 | 8.011 | 5.615 | 2 | |
| 7816.13 | 7817.21 | He I | 1/7 | 0.112 | 0.078 | 10 | |
| 8045.63 | 8046.85 | [Cl IV] | F1 | 0.864 | 0.588 | 4 | |
| 8233.21 | 8234.33 | H I | P 50 | 0.049 | 0.033 | 14 | |
| 8234.43 | 8235.55 | H I | P 49 | 0.062 | 0.042 | 13 | |
| 8235.74 | 8237.93 | H I | P 48 | 0.438 | 0.293 | 5 | |
| 8236.79 | | He II | 5.9 | | | | |
| 8237.13 | | H I | P 47 | | | | |
| 8238.61 | 8239.73 | H I | P 46 | 0.081 | 0.054 | 11 | |
| 8240.19 | 8241.33 | H I | P 45 | 0.072 | 0.048 | 12 | |
| 8241.89 | 8242.91 | H I | P 44 | 0.063 | 0.042 | 13 | |
| 8243.70 | 8244.87 | H I | P 43 | 0.082 | 0.055 | 11 | |
| 8245.64 | 8246.79 | H I | P 42 | 0.082 | 0.055 | 11 | |
| 8247.72 | 8248.87 | H I | P 41 | 0.087 | 0.058 | 11 | |
| 8249.97 | 8251.10 | H I | P40 | 0.082 | 0.055 | 10 | |

Table 20 – continued

| λ_0 | λ_{obs} | Ion | Identification | F | I | Error (%) | Notes |
|-------------|------------------------|----------|-------------------------|---------|--------|-----------|-------|
| 8252.40 | 8253.60 | H I | P 39 | 0.094 | 0.063 | 9 | |
| 8255.02 | 8256.01 | H I | P 38 | 0.076 | 0.051 | 10 | |
| 8257.86 | 8258.99 | H I | P 37 | 0.096 | 0.064 | 10 | |
| 8260.94 | 8262.13 | H I | P 36 | 0.112 | 0.075 | 8 | |
| 8264.28 | 8265.54 | H I | P 35 | 0.148 | 0.099 | 8 | |
| 8267.94 | 8269.10 | H I | P 34 | 0.122 | 0.082 | 8 | |
| 8271.93 | 8273.09 | H I | P 33 | 0.128 | 0.086 | 9 | |
| 8276.31 | 8277.48 | H I | P 32 | 0.122 | 0.082 | 8 | |
| 8281.12 | 8282.54 | H I | P 31 | 0.109 | 0.073 | 8 | |
| 8286.43 | 8287.41 | H I | P 30 | 0.124 | 0.082 | 8 | |
| 8292.31 | 8293.41 | H I | P 29 | 0.172 | 0.114 | 8 | |
| 8298.83 | 8299.93 | H I | P 28 | 0.183 | 0.122 | 7 | |
| 8306.11 | 8307.28 | H I | P 27 | 0.225 | 0.150 | 6 | |
| 8314.26 | 8315.43 | H I | P26 | 0.226 | 0.150 | 6 | |
| 8323.42 | 8324.57 | H I | P 25 | 0.250 | 0.166 | 6 | |
| 8333.78 | 8334.89 | H I | P 24 | 0.290 | 0.192 | 6 | |
| 8345.55 | 8346.70 | H I | P23 | 0.308 | 0.204 | 5 | |
| 8359.00 | 8360.20 | H I | P22 | 0.365 | 0.242 | 5 | |
| 8361.71 | 8362.92 | He I | V68 | 0.185 | 0.122 | 7 | |
| 8374.48 | 8375.72 | H I | P 21 | 0.372 | 0.246 | 5 | |
| 8392.40 | 8393.62 | H I | P 20 | 0.430 | 0.285 | 4 | |
| 8413.32 | 8414.72 | H I | P 19 | 0.680 | 0.449 | 4 | |
| 8421.95 | 8423.10 | He I | 6/18 | 0.030 | 0.020 | 16 | |
| 8433.85 | 8434.38 | [Cl III] | 3F | 0.007 | 0.005 | 34 | ? |
| 8437.96 | 8439.14 | H I | P 18 | 0.583 | 0.384 | 4 | |
| 8446.25 | 8447.02 | O I | 4 | 0.095 | 0.062 | 10 | |
| 8446.36 | | O I | 4 | | | | |
| 8446.76 | | O I | 4 | | | | |
| 8451.16 | 8452.23 | He I | 6/17 | 0.172 | 0.113 | 8 | |
| 8453.61 | | He I | 7/17 | | | | |
| 8467.25 | 8468.45 | H I | P 17 | 0.710 | 0.467 | 4 | |
| 8486.27 | 8487.54 | He I | 6/16 | 0.031 | 0.020 | 16 | |
| 8499.70 | 8500.99 | [Cl III] | 3F | 0.008 | 0.005 | 32 | |
| 8502.48 | 8503.74 | H I | P16 | 0.777 | 0.509 | 4 | |
| 8665.02 | 8666.03 | H I | P 13 | 1.831 | 1.186 | 5 | |
| 8680.28 | 8681.48 | N I | 1 | 0.064 | 0.042 | 24 | |
| 8727.13 | 8728.35 | [C I] | 3F | 0.116 | 0.075 | 20 | |
| 8733.43 | 8734.68 | He I | 6/12 | 0.088 | 0.057 | 20 | |
| 8736.04 | 8737.31 | He I | 7/12 | 0.032 | 0.021 | 34 | |
| 8747.15 | 8748.35 | He II | 6–24 | 0.040 | 0.026 | 34 | |
| 8750.47 | 8751.68 | H I | P 12 | 1.931 | 1.244 | 5 | |
| 8816.50 | 8817.83 | He I | 10/12 | 0.018 | 0.011 | 46 | |
| 8829.40 | 8831.00 | [S III] | 3F | 0.042 | 0.027 | 30 | |
| 8845.38 | 8846.68 | He I | 6/11 | 0.127 | 0.081 | 18 | |
| 8862.79 | 8864.02 | H I | P 11 | 2.402 | 1.536 | 4 | |
| 8996.99 | 8998.15 | He I | 6/10 | 0.173 | 0.110 | 16 | |
| 9014.91 | 9015.91 | H I | P10 | 2.608 | 1.654 | 4 | |
| 9063.29 | 9064.62 | He I | 4/8 | 0.196 | 0.124 | 14 | |
| 9068.60 | 9070.25 | [S III] | F1 | 72.752 | 46.011 | 2 | |
| 9123.60 | 9124.98 | [Cl II] | F1 | 0.150 | 0.095 | 16 | |
| 9210.28 | 9211.71 | He I | 6/9 | 0.236 | 0.148 | 14 | |
| 9213.20 | 9214.51 | He I | 7/9 | 0.056 | 0.035 | 26 | |
| 9229.01 | 9230.59 | H I | P 9 | 4.930 | 3.094 | 3 | |
| 9516.57 | 9518.13 | He I | 4/7 | 0.136 | 0.084 | 18 | |
| 9526.16 | 9527.65 | He I | 6 / 8 | 0.328 | 0.203 | 12 | |
| 9531.21 | 9532.52 | [S III] | F1 | 160.117 | 99.117 | 2 | |
| 9545.97 | 9547.52 | H I | P 8 | 5.845 | 3.616 | 3 | |
| 9824.13 | 9825.27 | [C I] | F1 | 0.226 | 0.138 | 14 | |
| 9850.26 | 9851.63 | [C I] | F1 | 0.747 | 0.457 | 8 | |
| 9982.46 | 9983.61 | O II | G[5] ₀ -2[6] | 0.150 | 0.091 | 16 | |
| 9988.54 | 9989.73 | O II | G[5] ₀ -2[6] | 0.132 | 0.080 | 18 | |
| 9990.08 | 9991.38 | O II | D[3] ₀ -0[4] | 0.260 | 0.158 | 12 | |
| 9991.48 | 9992.72 | O II | D[3] ₀ -0[4] | 0.127 | 0.077 | 18 | |

Table 20 – continued

| λ_0 | λ_{obs} | Ion | Identification | F | I | Error (%) | Notes |
|-------------|------------------------|------|----------------|-------|-------|-----------|-------|
| 10008.87 | 10010.09 | Ne I | | 0.131 | 0.080 | 18 | |
| 10027.70 | 10028.61 | He I | 6/7 | 0.390 | 0.237 | 10 | |
| 10031.20 | 10031.95 | He I | 7/7 | 0.135 | 0.082 | 18 | |
| 10049.40 | 10049.82 | H I | P 7 | 8.842 | 5.360 | 3 | |

- Kisielius R., Storey P. J., Davey A. R., Neale L. T., 1998, *A&AS*, **133**, 257
- Kisielius R., Storey P. J., Ferland G. J., Keenan F. P., 2009, *MNRAS*, **397**, 903
- Liu X. W., Storey P. J., Barlow M. J., Danziger I. J., Cohen M., Bryce M., 2000, *MNRAS*, **312**, 585
- Liu X. W., Luo S. G., Barlow M. J., Danziger I. J., Storey P. J., 2001, *Monthly Notices of the Royal Astronomical Society*, **327**, 141
- Luridiana V., Morisset C., Shaw R. A., 2015, *A&A*, **573**, A42
- McLaughlin B. M., Bell K. L., 2000, *Journal of Physics B Atomic Molecular Physics*, **33**, 597
- McNabb I. A., Fang X., Liu X. W., Bastin R. J., Storey P. J., 2013, *MNRAS*, **428**, 3443
- McNabb I. A., Fang X., Liu X. W., 2016, *MNRAS*, **461**, 2818
- Méndez-Delgado J. E., Esteban C., García-Rojas J., Henney W. J., Mesa-Delgado A., Arellano-Córdova K. Z., 2021, *MNRAS*, **502**, 1703
- Mendoza C., Zeippen C. J., 1982a, *MNRAS*, **198**, 127
- Mendoza C., Zeippen C. J., 1982b, *MNRAS*, **199**, 1025
- Mendoza C., Zeippen C. J., 1983, *MNRAS*, **202**, 1981
- Morisset C., 2013, pyCloudy: Tools to manage astronomical Cloudy photoionization code (ascl:1304.020)
- Nicholls D. C., Dopita M. A., Sutherland R. S., 2012, *ApJ*, **752**, 148
- Nicholls D. C., Dopita M. A., Sutherland R. S., Kewley L. J., Palay E., 2013, *ApJS*, **207**, 21
- Osterbrock D. E., 1974, *Astrophysics of gaseous nebulae*. W.H. Freeman
- Peña-Guerrero M. A., Peimbert A., Peimbert M., Ruiz M. T., 2012, *ApJ*, **746**, 115
- Peimbert M., 1967, *ApJ*, **150**, 825
- Peimbert M., 1978, in Terzian Y., ed., *IAU Symp Vol. 76, Planetary Nebulae*. pp 215–224
- Peimbert M., Costero R., 1969, *Boletín de los Observatorios Tonantzintla y Tacubaya*, **5**, 3
- Peimbert A., Peimbert M., 2013, *ApJ*, **778**, 89
- Peimbert M., Torres-Peimbert S., 1983, in Aller L. H., ed., *IAU Symp Vol. 103, Planetary Nebulae*. pp 233–242
- Peimbert A., Peña-Guerrero M. A., Peimbert M., 2012, *ApJ*, **753**, 39
- Peimbert A., Peimbert M., Delgado-Inglada G., García-Rojas J., Peña M., 2014, *Rev. Mex. Astron. Astrofis.*, **50**, 329
- Peimbert M., Peimbert A., Delgado-Inglada G., 2017, *PASP*, **129**, 082001
- Pequignot D., Aldrovandi S. M. V., 1976, *A&A*, **50**, 141
- Podobedova L. I., Kelleher D. E., Wiese W. L., 2009, *Journal of Physical and Chemical Reference Data*, **38**, 171
- Porter R. L., Ferland G. J., Storey P. J., Detisch M. J., 2012, *MNRAS*, **425**, L28
- Porter R. L., Ferland G. J., Storey P. J., Detisch M. J., 2013, *MNRAS*, **433**, L89
- Ramsbottom C. A., Bell K. L., 1997, *Atomic Data and Nuclear Data Tables*, **66**, 65
- Ratag M. A., Pottasch S. R., Dennefeld M., Menzies J., 1997, *A&AS*, **126**, 297
- Rauch T., 2003, *A&A*, **403**, 709
- Schoening T., Butler K., 1998, *A&AS*, **128**, 581
- Schoening T., 1997, *A&AS*, **122**, 277
- Stanghellini L., Shaw R. A., Villaver E., 2008, *ApJ*, **689**, 194
- Stasińska G., 1978, *A&A*, **66**, 257
- Sterling N. C., Porter R. L., Dinerstein H. L., 2015, *ApJS*, **218**, 25
- Storey P. J., Hummer D. G., 1995, *VizieR Online Data Catalog*, p. VI/64
- Storey P. J., Zeippen C. J., 2000, *MNRAS*, **312**, 813
- Storey P. J., Sochi T., Badnell N. R., 2014, *MNRAS*, **441**, 3028
- Storey P. J., Sochi T., Bastin R., 2017, *MNRAS*, **470**, 379
- Tayal S. S., 2004, *A&A*, **426**, 717
- Tayal S. S., 2011, *ApJS*, **195**, 12
- Tayal S. S., Gupta G. P., 1999, *ApJ*, **526**, 544
- Tayal S. S., Zatsarinsky O., 2010, *ApJS*, **188**, 32
- Tsamis Y. G., Péquignot D., 2005, *MNRAS*, **364**, 687
- Wesson R., Liu X. W., Barlow M. J., 2003, *MNRAS*, **340**, 253
- Wesson R., Jones D., García-Rojas J., Boffin H. M. J., Corradi R. L. M., 2018, *MNRAS*, **480**, 4589
- Wiese W. L., Fuhr J. R., Deters T. M., 1996, *Atomic transition probabilities of carbon, nitrogen, and oxygen : a critical data compilation*. NIST
- Yuan H. B., Liu X. W., Péquignot D., Rubin R. H., Ercolano B., Zhang Y., 2011, *MNRAS*, **411**, 1035
- Zhang Y., Liu X. W., Wesson R., Storey P. J., Liu Y., Danziger I. J., 2004, *MNRAS*, **351**, 935
- Zhang Y., Liu X. W., Liu Y., Rubin R. H., 2005, *MNRAS*, **358**, 457
- van Hoof P. A. M., 2018, *Galaxies*, **6**, 63

This paper has been typeset from a $\text{\TeX}/\text{\LaTeX}$ file prepared by the author.